THESIS

ONE-DIMENSIONAL EFFECTIVE CONTINUUM MECHANICS MODELS OF BRAIDED AND TRAPEZOIDAL WIRES

Submitted by

Mohammed K. Alkharisi

Department of Civil and Environmental Engineering

In partial fulfillment of the requirements

For the Degree of Master of Science

Colorado State University

Fort Collins, Colorado

Fall 2017

Master's Committee:

Advisor: Paul Heyliger

Suren Chen
Chris Weinberger

ABSTRACT

ONE-DIMENSIONAL EFFECTIVE CONTINUUM MECHANICS MODELS OF BRAIDED AND TRAPEZOIDAL WIRES

As the use of wires in different engineering applications increases, investigation into and better understanding of the wire's behavior become more important. Over the past years, heavy work has been done to study the mechanical and dynamical behavior of wires using analytical, experimental, and finite element models. This attention explains the importance of such a structure. However, studying such a structure is more challenging than with other ordinary structures, due to the nonlinearity of the geometry.

In this work, the axial elastic behavior was studied using linear three-dimensional finite element Fortran 77 code. The wire was discretized, element matrices were built, and varying boundary conditions were applied to find the four elastic coefficients of the global matrix: pure tensile stiffness, two coupling terms between the tensile and torsional stiffness. Couple action appears when there is a twist in the wire, for that varying twist angles (0°, 5°, 10°, 15°, 20°, 25°, and 30°) were used to check their effect on the stiffness. To validate the model used, a simple straight wire rope (1+6) of known behavior was tested using same approach and twist angles, and then compared with 7 existing analytical models available in literature. Results showed a good agreement with the finite element model, which indicates that the approach used to solve for the trapezoidal wire was reliable and valid. The results showed that the trapezoidal wire is stiffer than the simple straight wire rope and exhibited extensional and torsional coupling behavior values,

which can be critical in the design process of these structures. This model can also be used to decrease the high costs associated with experimental tests needed to determine its behavior.

The method was extended, as, to evaluate the integrity of such a structure, it was essential to conduct a free vibration analysis using a one-dimensional finite element approximation for the trapezoidal wire as well as for the simple straight wire rope, which had not been done before, to investigate the extensional and torsional behavior of the motion of these wires. First, an aluminum straight bar was tested by solving the mass and stiffness matrices using 2-, 4-, 8-, and 16-element approximations, and the convergence was checked against the known exact axial and torsional frequency solutions. The 16-element approximation was applied to both the trapezoidal and the simple straight wire rope with all the lay angles considered. The coupled extensional and torsional vibration for these wires was solved using closed-form equations for the mass matrices; with these and the stiffness matrices constructed, the eigenproblem was solved to find the frequencies and the corresponding mode shapes. The two types of displacement, axial and torsional, were found in each frequency while having coupled stiffness. The simple straight wire rope behaved similarly to the trapezoidal wire, but with relatively lower frequencies. Which conclude that it is important to the design, safety, and monitoring, depending on the application for which these wires are used, that the coupled frequencies suggested be considered and studied carefully.

ACKNOWLEDGMENTS

I would like to express my appreciation to all the people who helped me to complete this research. My sincere gratitude goes to Prof. Paul Heyliger for giving me the opportunity to work with him; for his constant guidance, encouragement, and support, without which this work would have not been completed. Also, I would like to thank my committee, Prof. Suren Chen and Prof. Chris Weinberger, for their assistance and advice.

A special and generous thanks to my father, my mother, and all my family members for their continuous support. I am fully indebted to my beloved wife Hessah Alsaleem for her patience, help, and encouragement.

Finally, it is a pleasure to acknowledge my thanks to the Saudi government and Qassim University for their financial support and cooperation for affording me the privilege of pursuing a Master of Science degree in the Civil Engineering Department at Colorado State University.

TABLE OF CONTENTS

LIST OF TABLES

LIST OF FIGURES

CHAPTER 1: INTRODUCTION

1.1 Overview

Over the past years, with the increase in the use of wires in different engineering applications, a better understanding of their behavior is essential, so, much work has been done to study the mechanical and dynamic behavior of spiral strands and wire ropes using analytical, experimental, and finite element (FE) models. Such attention bespeaks the importance of such a structure. A spiral strand can be defined as multiple layers of helical wires wound around a straight wire, whereas a wire rope is typically six wires wound around a straight core wire. Hobbs and Raoof (1996) observed that the difference between spiral strands and wire ropes is that the spiral strand has a simpler helical path for each wire around its center wire, while the wire rope has more complex and double helical paths in strands which are themselves helically constructed.

Wire strands and ropes are widely used in many engineering applications, for instance, in suspension bridges, aerial ropeways, mine hoists, overhead electrical conductors in transmission lines, etc., because of their ability to take large axial loads (a dominant advantage in comparison with small torsion or bending stiffness), their high strength over weight, and their ability to take advantage of their material in a very effective way. Indeed, their mechanical and dynamic behavior depend on their geometry, material, and the lay configurations of each wire.

Experiments on large-diameter strands need expensive and huge devices. It is important for designers to have tools with which to determine the axial elastic stiffness of these kinds of structures. For this purpose, there are many analytical models based on different assumptions, including, for example, purely tension wires, Poisson's ratio effects, curved beam theory, friction effects and variations in core radius, on a single layer or multilayers strands with a single helix or multihelix configuration, and testing different lay angles α. Also, with the development of finite

element modeling, comparing the early analytical models made it possible to study more and more interesting phenomena, including vibration analysis. Related and most important models were introduced and are presented in the literature review in chapter 2. The complexity starts when the wire has a twist along its length, which means extensional and torsional coupling action appears in the stiffness matrix of the wire.

A new aluminum composite conductor core with trapezoidal outer wires and a polymer hybrid composite core was designed as a solution to a major problem in the electrical overhead conductors used in the transmission lines; the current metal conductors cause a limitation in the distribution capacity when there is an increase in the demand because of heat, which causes expansion, which results in end of sag. In addition, if there is an excessive sag, the risk of human injury and property damages will increase significantly. Furthermore, in a side note, Alawar, Bosze, & R. (2007) assessed this new wire under high temperature (100°C to 180°C) and found that the core lost only 10% from room temperature, and studied creep under 150°C and stated that the results were insignificant since the change in sag was only 0.35 mm for a typical span length.

Nevertheless, in this work the global axial mechanical behavior of the new trapezoidal wire (Figure 1.1) is the focus, which leads to conducting a vibration analysis. The study measured the change of the wire behavior within the change of the lay angles, which is the angle it takes a full wire to turn around a center straight wire, the angles used between 5° and 30° which covers the most practical lay angles. The wire was first meshed using AutoCAD to model in detail all the geometric aspect of the wire and then conduct a three-dimensional finite element analysis using a Fortran 77 code. To validate this methodology, a well-known simple straight wire rope's (Figure 1.2) mechanical behavior was analyzed using the same process and methodology and its results

then compared with 7 other known analytical models. The coupling behavior resulting from the axial load where the twisting angle (lay angle) exists was the focus of the study.

Figure 1.1 Trapezoidal wire.

Figure 1.2 Simple straight wire rope.

In addition, free vibration analysis using one-dimensional finite element approximation for the trapezoidal wire and the simple straight wire rope was conducted after finding the mass matrices and stiffness matrices, as mentioned before, for each lay angle α studied (0°, 5°, 10°, 15°, 20°, 25°, and 30°); the natural frequencies and the corresponding mode shapes were found using Matlab function. The effect of coupling (extensional and torsional) behavior in the vibration analysis is of interest to this research, as it has not been studied before for wires.

The results for the mechanical behavior of the trapezoidal wire were better than for the simple straight metal wire rope and proved it is a stiffer wire, that can be relied on in many engineering applications. The simple straight wire rope's elastic stiffness was satisfactory in comparison with the 7 analytical models for all lay angles.

It is also important for designers to study the significance of the coupling action in the trapezoidal wire and the simple straight wire rope in solving the free vibration analysis, which showed two types of displacement in a wire with a twist, primarily axial with torsional or reverse. In comparisons of the trapezoidal wire to the simple straight strand, the trapezoidal had better results, indicating that it can be used in more applications.

1.2 Mechanical Behavior of Wires

In general, wires are helically designed and despite how many layers or the section shape they have, their global axial behavior for linear elastic analysis will be a coupling between tension and torsion as in (1):

$$\begin{Bmatrix} F_z \\ M_z \end{Bmatrix} = \begin{bmatrix} k_{\varepsilon\varepsilon} & k_{\varepsilon\theta} \\ k_{\theta\varepsilon} & k_{\theta\theta} \end{bmatrix} \begin{Bmatrix} u_{z,z} \\ \theta_{z,z} \end{Bmatrix} \quad (1)$$

where F_z, M_z, $u_{z,z}$, $\theta_{z,z}$, $k_{\varepsilon\varepsilon}$, $k_{\varepsilon\theta}$, $k_{\theta\varepsilon}$, and $k_{\theta\theta}$ are the axial force (F_z,), the axial twisting moment (M_z), the global axial strain ($u_{z,z}$,), the global twist angle per unit length ($\theta_{z,z}$), the global

pure tensile stiffness ($k_{\varepsilon\varepsilon}$), the global coupling stiffness terms between the tensile ($k_{\varepsilon\theta}$) and the torsional ($k_{\theta\varepsilon}$), and the global torsional stiffness ($k_{\theta\theta}$). Note that the equations used in this research follow the notations of Ghoreishi, Messager, Cartraud, & Davies (2007).

It should be mentioned that the coupling terms in the stiffness matrix should be symmetrical to satisfy the Maxwell Betti reciprocal theorem, which is a basic law in conducting a linear elastic structure analysis (more discussion on which will be presented in chapter 4).

This research focus will be on two wires: (1) the new trapezoidal wire, composed of two layers of trapezoidal-section aluminum helical wires wound around a center wire with circular section composed of two different materials: carbon/glass-fiber polymer composite, as shown in Figure 1.1. And (2) the simple straight wire rope, which contains one layer of six helical wires wound around a center wire, all of them having a circular section and being made of similar material (i.e., steel), as shown in Figure 1.2. The stiffness matrix of the trapezoidal wire has not yet been solved.

1.3 Dynamic Behavior of Wires

As is well known, due to its geometry, when a wire (even a small wire) has a twist, the tension will not only result in extension of the wire, it will have a rotation as well; likewise, when it has a torque load it will produce not only rotation, but extension also (Samras, Skop, & Milburn, 1974). This behavior of the stiffness matrix has been extensively studied, along with the effects of such an aspect on a structure like wire. Free-vibration-analysis eigenvalues (natural frequencies) and eigenvectors (mode shapes) can be solved after finding the stiffness and mass matrix for linear structure analysis. In this work, the frequencies and the corresponding modes shape were solved for the new trapezoidal wire and the simple straight wire rope as it has not been solved before to study the effect of the coupled stiffness on the oscillation of such a structure.

1.4 Objectives

There are many goals in this work. It starts with studying the complex geometry of these structures (trapezoidal wire and simple straight wire rope) using a three-dimensional finite element model; accurate discretization of the structure is essential for such a method. Then building the element matrices after finding out the elastic properties. The models will be solved using different boundary conditions, to find the global axial stiffness matrix for lay angles between 0° and 30° for the new trapezoidal wire using Fortran 77 code. To validate the results, the known mechanical behavior of simple straight wire rope was used on the same three-dimensional finite element code and application, and its results will be checked with 7 existing analytical models. Next, free vibration analysis will be used to study the extensional and torsional behavior of the trapezoidal wire and the simple straight wire rope; an aluminum bar with approximately the same radius as the trapezoidal wire will be used. Mass matrices will be constructed for each structure studied. The dynamic stiffness element matrix will be computed for all lay angles specified for both the trapezoidal and the simple straight wire rope, along with the bar stiffness, to find the natural frequencies and the mode shapes to confirm the method used and compare it with known exact solutions.

1.5 Thesis Organization

This thesis contains 5 chapters and an appendix. The first chapter is an introduction with 5 parts: (1) an overview about this thesis, (2) a brief peak of wire history and its uses, (3) a general description of the wires' overall mechanical behavior, (4) overall dynamic behavior of wires, and (5) a list of the objectives of this thesis. Chapter 2 is a detailed literature review divided into 4 parts: the first shows the analytical and experimental models; the second, the finite element models; the third shows the free vibration analysis for wires; and the fourth, a statement of the

significance of this research and the methods used. chapter 3 is divided into 4 main sections: (1) an overview, (2) a discussion of how the global stiffness matrix was obtained for the trapezoidal wire and the simple straight wire rope using a three-dimensional finite element method, (3) a listing of the 7 analytical models for the simple straight wire rope, and (4) the free vibration analysis for the aluminum bar, the trapezoidal wire, and the simple straight wire rope. Chapter 4 shows the results and discussion on the method applied in chapter 3, also divided into 3 main sections: (1) an overview, (2) the mechanical behavior of both the trapezoidal wire and the simple straight wire rope, and (3) the dynamic behavior of the aluminum bar, the trapezoidal wire, and the simple straight wire rope. Chapter 5 is a conclusion, which lists the study findings and possible future work or improvement on this research. At the end there is appendix containing the stiffness values of the analytical models for the simple straight wire rope.

CHAPTER 2: LITERATURE REVIEW

2.1 Background

There are many experimental and analytical models focused on the description of the mechanical behavior of a single straight isotropic strand subjected to axial load while knowing the wire's material and geometry, which are partially described by Feyrer (2015). The focus of the authors was to find the global response of wire ropes—the axial, bending, and torsion stiffness—as well as the local deformation of individual wires, which are critically related to the fatigue and damage behavior of the wire ropes (Xiang et al., 2015). Lee (1991) introduced a geometrical technique that can work with any cable with axisymmetric strands and noted that this damage is closely associated with the geometrical properties of the individual wires of which a rope is constructed. The degree of damage depends upon the geometrical and spatial configuration of the wires as well as their positions within the rope; Lee (1991) noted that a thorough understanding of the geometrical properties is required to model the deformation and strain components along individual wires within a rope under operating conditions. Later, other mathematical models were created and are now available to predict the mechanical behavior of a two- and three-layered isotropic straight strand subjected to axial loads while knowing the wire's material and geometry.

Later, with the development of advanced finite-element methods, many scholars investigated the mechanical response of a simple straight wire and two- and three-layered straight wire using different approaches and different software (to save time and cost of these analytical models and experimental models, presented before became available). The finite element method was used also for the design as well as for the investigation of the behavior of wire strands. In addition, using finite elements gave the advantage of searching many different wire geometry configurations and materials, under various assumptions.

However, very few studies have researched the vibration phenomena, including the natural frequencies and the normal modes for coupled extensional torsional in wires.

To follow precisely what research has been done, this chapter is divided into four sections: the first describes the analytical and experimental models, the second shows the finite element models followed, the third is a vibration analysis, and in the fourth a description of the significance of this study is presented.

2.2 Analytical and Experimental Models for Wires' Mechanical Response

The first model dates back to the early 1950s, which was a fiber model by Hruska (1952a, 1952b). His model was the simplest; he accounted for the tension response of each wire and ignored its bending and torsion (clamping conditions). He assumed zero end rotation and the contact mode was radial; however, he ignored the radial contraction as well as the friction (Cardou & Jolicoeur, 1997), so he did not investigate the actual contact stresses. This model was later extended by R. Knapp (1975) with a rigid core. It should be noted that bending and torsion cannot be negligible because newer models considered the bending and torsion response and explained why it needed to be included (Xiang et al., 2015). So, in the McConnell and Zemke (1982) model, they included the torsional stiffness for each cable around the center cable.

As in McConnell and Zemke's (1982) model, the next analytical models were based on beam theory assumptions, which were modeled using (Love, 1906) curved beam equations, where they dealt with each wire individually by assuming it to be a helically curved rod but making different assumptions about the geometry or even the contacts of the interwire (Anne Nawrocki & Labrosse, 2000). Machida & Durelli (1973) also studied the mechanical response when they added the bending and torsion stiffness to the global stiffness matrix, as in Knapp's (1975) model. Knapp

(1979) extended the work by examining the effect of changing the core radius due to the layers' pressure.

Costello and Phillips' (1976) model also considered the bending and torsion stiffness of the wire while ignoring the friction force and contact deformation. The model was developed on a nonlinear theory for a simple straight wire with a soft core or without a core; due to the Poisson ratio, the effect of the angle and radius of the cable were included, and forces from lateral contact were calculated on the assumption that the cable cross-section is an ellipse, which entails a smaller lay angle, normally less than 30 degrees. Cable strain was neglected while it will appear from only changing the helix angle; the last assumption was neglected in Phillips and Costello's (1985) model (Cardou & Jolicoeur, 1997). Velinsky (1985) extended it to a cable with a core, taking into account the Poisson ratio (radial contraction) with small lay angles as well for the bending and torsion stiffness of the wire. This model was the first to compute the response of a multi-strand construction. Moreover, this model calculated the tension and torque for a straight wire due to a uniform tension and torsion; then the wound strand's tension and torque that resulted, due also to elongation and torsion, was approximated by exactly the same mechanical relation computed for the straight wire. The effect of curvature changes of the wound wire was included in this model by an approximation that accounted for the bending in the plane for the straight wire around a cylinder (Elata, Eshkenazy, & Weiss, 2004). Phillips and Costello (1985) continued the work by generalizing Velinsky's (1985) model for any type of cable with an independent wire rope core; this model neglected the friction between the wires as well. After that, Costello (1997) developed a linearized theory, including a study of the effect of twist and curvature. Kumar and Cochran (1987) linearized Costello's (1997) theory and included the Poisson ratio, and that resulted in finding a closed-form expression for the stiffness matrix terms. By using a metallic material for

the wire core, Kumar and Botsis (2001) extended Kumar and Cochran's (1987) work to obtain an analytical expression for the maximum contact stress found in the multilayered strands (Ghoreishi, Messager et al., 2007). Jiang (1995) developed a general formulation to be applied to more complex wire geometries for one-layered as well as multilayered wires. Huang (1978) investigated the contact mode conditions either radially or laterally for the simple straight wire. While the Poisson effect is considered and local contact deformation is neglected, it was shown that radial contact appeared to be prevalent, even if no gap exists between the wire's layers (Ghoreishi Messager et al., 2007). Utting and Jones (1987a, 1987b) continued Costello's analysis to include wire flattening, which is contact deformation and friction. The results proved that these phenomena have almost no effect on estimates of the global cable response (Ghoreishi, Messager et al., 2007).

Jolicoeur and Cardou (1991) studied the response of a simple straight wire by Costello and Phillis' (1976) model and the estimated result of Hruska's (1952a, 1952b) model, and the study found that the fiber model is not appropriate when twisting moment and angle have to be taken into consideration; however, the thin-rod model showed good results comparing the stiffness terms with the experimental results in Utting and Jones (1987b).

Ramsey (1988) stated that more analysis should be done specifically for the wire twist, so he derived new constitutive equations using an accurate theory. Then, Ramsey (1990) revised his earlier work, leading to a non-zero distributed moment component in the radial direction (Cardou & Jolicoeur, 1997).

For a cable with a rigid core, Sathikh, Moorthy, and Krishnan (1996) derived a closed-form symmetric linear elastic model, using discrete thin-rod theory because most of the earlier models lack symmetry when the bending and torsion terms are included and he compared his result with these models, such as Ramsey's theory as well, with the experimental result obtained before.

Labrosse (1998) presented a new analytical approach to predict the overall behavior of simple straight wires subjected to tension, bending, and torsion. In this model, the Poisson ratio effect is neglected while relative motions between core and wires are considered (Ghoreishi, Messager et al., 2007).

Elata et al. (2004) simulated a new model for the mechanical response of a wire rope with an independent wire rope core under axial loads and axial torque. In contrast to the earlier models, where the effective response of wound strands was considered, this model considers the complete double-helix configuration of the wires within the wound strand and relates the wire level stress to the applied overall load at the rope level. Only axial stiffness is considered, but the wires are subjected to loads on their lateral surface, applied by adjacent wires; as a result, the accuracy of this model increases when the number of wires increases (Ghoreishi, Messager et al., 2007). Elata et al.'s (2004) major concern was to analyze the effect of a double-helix configuration. However, this model does not lead to closed-form equations.

There are many authors who have worked on such structures having a large number of components. As Raoof and Hobbs (1988) stated, for such cables the bending moment and torque were not considered. These authors developed models to find the global elastic constant, knowing the material and geometry of the structures. These models fall into two groups: (1) semicontinuous models developed only for metallic cables, and (2) models for synthetic cables (Ghoreishi, Cartraud, Davies, & Messager, 2007).

For semicontinuous models, a method called homogenization is used for multilayered cables, and it is basically changing a system composed of identical repetitive elements into one made of continuous material; these models are in contrast to the thin-rod models. Hobbs and Raoof (1982) were the first to apply this approach to their cable model, and they extended it further

(Raoof, 1983). This model replaced each wire layer with a thin cylindrical orthotropic layer, to be in a plane state of stress. Four elastic constants are important for composite laminates: two are related to the properties of the wires and two are related to the contact stiffness between the wire layers (Cardou & Jolicoeur, 1997). The whole cable was then treated as a discrete concentric orthotropic cylinder set (Ghoreishi, Cartraud et al., 2007). That led Raoof and Hobbs (1988) to calculate the axial stiffness, as well as the torsional stiffness (Raoof and Hobbs, 1989), and that work was extended for two decades by Raoof and Kraincanic (1995), and Mohammed and Ivana (1995). Using the same idea but replacing each layer with an orthotropic cylinder, of transversely isotropic material, first Blouin and Cardou (1989), then Crossley, Spencer, and England (2003), Claude and Alain (1996), and then Crossley, England, and Spencer (2003) extended the work, taking into account that such method is applied when the number of wires is larger than six. The cylinder thickness is arbitrary, so, for the three-dimensional model, five elastic constants are needed instead of four (Cardou & Jolicoeur, 1997). These models included the friction between components, but some elastic constants are derived from contact mechanics because the layers are considered to be circular cross-sections (Ghoreishi, Cartraud et al., 2007). However, Jolicoeur (1997) studied and compared Raoof's (1983) and Blouin and Cardou's (1989) models, and indicated that the previous cylinder model is easier and simpler for tension or torsion loads; however, using this approach when there is bending will result in failing to get the bending stiffness (Spak, Agnes, & Inman, 2013). Raoof and Kraincanic (1994) have also compared the semicontinuous models versus the thin-rod model and indicated that the thin-rod method was more reliable when the wire diameter is small, whereas, for the semicontinuous models it would be better with a larger number of wires (Xiang et al., 2015).

Moreover, some models for analyzing synthetic cables were presented. The simplest model is that of Raoof (1991). While still accounting for tension and neglecting bending, torsion, friction, and contact, this approximation is acceptable for monotonic axial loading (Ghoreishi, Cartraud, et al., 2007). Leech, Hearle, Overington, and Banfield (1993) presented a quasi-static analysis using computer codes for fiber ropes and splices to predict the ropes' properties; from their dependence on elongation and twist they computed the tension and torque. Beltran, Rungamornrat, and Williamson (n.d.) and Beltran and Williamson (2009) developed models that are very similar to that of Leech (although Leech focused on a damaged model, to take into account the degradation of rope properties as a function of loading); these models are also implemented in a computer program (Ghoreishi, Messager, et al., 2007).

For two dimensions, recently, Argatov (2011) presented a refined discrete mathematical model for a simple straight wire, and this model took the effect of the Poisson ratio and the contact deformation into consideration, and found the wire stiffness and local contact stress; this model assumed a plane strain to formulate the two-dimensional problem (Frikha, Cartraud, & Treyssède, 2013).

Recently, Ghoreishi, Cartraud, et al. (2007) did two tests on two structures of a fibrous cable with a large number of twisted components subjected to axial loads; using their model the axial stiffness of the structures has been predicted. They continued their work in Ghoreishi, Davies, Cartraud, and Messager (2007); at the end of their research they came up with two closed-form analytical models that can be used to analyze synthetic cables.

It should be noted that it is difficult to complete an analytical investigation of the mechanical response for a cable because the kinematics of each individual wire is very complex. To complete such a study, it is essential to assume the kinematics of the wire and then compute

the mechanical behavior for the structure as a whole and, after that, test the consequences of these assumptions by considering their effect on the validity of the equilibrium equation (Love, 1906).

2.3 Finite Element Models for Wires' Mechanical Response

In the 1970s, Carlson, Kasper, and Tucchio (1973) were the first to model armored wire using the finite element method; they modeled the wire and its connections using bar elements (Ghoreishi, Messager, et al., 2007). A study of the damping isolators for multiconductor cable was presented by Cutchins, Cochran, Guest, Fitz-Coy, and Tinker (1987); this model used a six-nodal solid element and the connections were simulated with springs (Ghoreishi, Messager, et al., 2007). A small segment length of the cable was modeled for a simple straight wire only to optimize the geometry by Chiang (1996); the model investigated the main impact design factors, including the radius of the core, the radius of the wire, the helical angle, and the boundary conditions. The previous models used volumic finite elements, which are not applicable to investigate all the interwire mechanical behavior; and indeed to model a cable accurately, it is essential to have a large number of elements (Nawrocki & Labrosse, 2000). Jiang, Yao, and Walton (1999) presented a concise finite element model; taking advantage of the cable and loading symmetry, the model used three-dimensional solid brick elements. This model accounted for tension, shear, bending, torsion, contact, friction, and possible local plastic yielding when axially loaded. The model showed excellent agreement with the analytical model by Costello (1978) as well as the experimental work by Utting and Jones (1987a, 1987b). Jiang, Henshall, and Walton (2000) extended the work by applying it for a three-layered straight strand. However, this model cannot be applied for the bending case, nor for a very complex load. Using a simple straight wire, Jiang, Warby, and Henshall (2008) studied the statically indeterminate contact problem when the wire is

axially loaded; the results of this study showed that contacts can happen at all possible contact points if the wire is under tension and both ends restrained against rotation.

Rope stress was calculated using the finite element method by Wehking and Zieglen (2004). Messager and Cartraud (2008) took advantage of the helical symmetry and used the semicontinuous (or the so-called homogenization) theory of periodic slender domain to find the elastic behavior from a three-dimensional concise finite element model that is free of the displacement assumption. A cable with large perturbations with interwire friction and deformation of the wire cross-section was modeled by Durville (1998); however, this model has no experimental validation (Nawrocki & Labrosse, 2000). Nawrocki and Labrosse (2000) presented a finite element model to predict the behavior of simple straight wire rope strands, which allows the study of all the possible interwire behaviors. They investigated the contact conditions in axial loading and in combined axial and bending load, which was an extension of the work done by Nawrocki (1997), where a one-dimensional curved beam element was investigated for a simple straight wire. Michel, Anne, and Ted (2000) analyzed the frictional damping properties of axially loading on one-layered cables, such as a simple straight wire rope, and investigated the quantity of energy dissipated through friction due to motions between wires when loading.

In an excellent work done by Ghoreishi, Messager, et al. (2007), they presented a three-dimensional finite element model and used it as a reference to compare the validity domain of the analytical models, i.e., those of Hruska (1952a, 1952b), McConnell and Zemke (1982), Machida and Durelli (1973), Knapp (1979), Kumar and Cochran (1987), Ramsey (1988, 1990), Sathikh, Moorthy, and Krishnan (1996), Costello (1997), and Labrosse (1998). For lay angles below 20 degrees of the nine linear elastic models of the simple straight wire rope subjected to axial load, the compared finite element model showed a satisfactory estimation; however, it showed that the

analytical models have limitations due to their assumptions, for example, that the simple strand is actually assumed to be linear elastic (Chen, Meng, & Gong, 2017).

Because most of the analytical models presented depended on neglecting the friction effect and beam theory, Erdönmez and Ímrak (2009) created a three-dimensional model for a wire strand considering friction and sliding effects. Using a simple straight two-layered wire rope, Páczelt and Beleznai (2011) studied the possible interwire motions, contact, and friction between the wires as well as the Poisson ratio and wear effect between the elements by developing the p-extension concept in the finite element mesh of a simple straight two-layered cable. This model considered tension, torsion, and bending loading, and it showed accuracy when they compared it with several analytical models. Erdönmez and Ímrak (2011) presented an accurate three-dimensional solid modeling that can be used for finite element analysis by the new methodology of defining and modeling the nested helical wire ropes; they presented the parametric equations for single and nested helical wire ropes. Prawoto and Mazlan (2012) introduced a simple theory and computational, mechanical, and metallurgical characteristics of wire rope to find their mechanics under axial loading. Wang, Zhang, Wang, and Ge (2012) presented a three-dimensional finite element analysis for a hosing rope and three-layered strand subjected to fretting fatigue and stress. The study showed that different wires in the rope or strand and distinct material in the analyses generate different parameters of the fretting fatigue and stress. This study's results showed agreement with the results of experimental work done previously. An investigation by Frikha, Cartraud, and Treyssède (2013) was performed to study the behavior of a simple straight wire rope under tension load considering their translation invariance and applying the homogenization theory based on an asymptotic expansion. Stanova, Fedorko, Fabian, and Kmet (2011a, 2011b) presented

parametric equations to generate arbitrary multilayered strand ropes with circular sections and apply it to a finite element application (Stanova, Fedorko, Kmet, Molnar, & Fabian, 2015).

For pure bending, Jiang (2012) presented a concise three-dimensional finite element model for a straight wire strand, before applying it to the periodic artificial cross-sectional end boundaries. Jiang created a bending symmetric condition, which was accurate. For bending moment versus bending curvature, the models had satisfactory results when compared with the analytical results of Costello's (1997) model theory. In addition, this model is able to show the progressive nonlinear plastic behavior of the strand.

2.3 Models for Wires' Dynamic Response

The vibration analysis of tight strings started by Taylor, D'Alembert, Euler, and Bernoulli, Bernoulli studied the transverse vibration of a uniform wire clamped at one end. After 50 years, Euler and Bernoulli solved the natural frequencies as inform of series that were infinite (Irvine, 1974). After the use of partial differential equations, in 1788, Lagrange had come up with a solution for the vibration of a tight wire that is fixed and both ends. The general motion equations were first introduced by Largrange in 1760 and then improved in Mecanique Analytique in 1788. The general force action was included in the Cartesian partial equations used for that wire and modified for vertical wires; this is was a huge contribution in the wire's vibration analysis, made by Poisson in 1820 (Irvine, 1974). It should be noted that until this point in history, the free vibration of wires with sag had not been studied. In 1851, Rohrs found vertical vibration approximation for the fixed wire with a very small sag compared to its span. Roith (1868) did similar work to obtain the exact solution for symmetric and antisymmetric vertical vibration, and the work on wires vibration did not have any major improvement until Karman and Rannie (1941) derived symmetric and antisymmetric vertical vibration of three-span wire. For the same wire span

Vincent (1965) continued the work by including the elastic properties in the model, more extensive study taking the same approach by Bleich (1950); however, he was concerned about including a sag ratio of 1:10, so the wire elasticity was not appreciable (Irvine, 1974). Pugsley (1949) was the first to solve the natural frequencies for the first three modes of a wire using empirical theory and he tested the result of changing the sag-to-span ratio from 1:10 to 1:4. Saxon and Cahn made a major improvement in the in-plane vibration theory, where they found solutions that effectively decreased the previous results for a small sagged wire and yielded very good results for the larger sag-to-span ratio. An interesting aspect of these studies at that time was that no one had searched the discrepancy when the sag-to-span ratio goes to zero; as most of the theories assumed a small sag, the first mode would primarily have a vertical motion (Irvine, 1974). Most of this historical review was presented in a classic paper by Irvine, who also did a remarkable study based on a linear theory for the free vibration analysis for uniform wires; but with a sag-to-span ratio of 1:8 or less, he concluded that the analysis depended on the wire's geometry and elasticity parameters. An experimental study needs to be done to prove the validity of his theory. It can be clearly seen that these earlier models were limited by the lack of the advanced mathematical methods available today (Thai, Kim, & Lee, 2017). Other recent analytical work has focused more on other things, like the increase of nonlinear interactions, as in Rega's (2004) paper or the study of the increase in temperature on the wire's sag by Lepidi & Gattulli (2012). In addition, most of these methods studied the axial deformation only.

Samras et al. (1974) studied the coupled extensional torsional and found the equation for it solved the frequency equations under four different boundary conditions. The study derived the coupled extensional and torsional motion equations, and the frequencies were computed for a wire stretching from the ocean floor to the surface. These frequencies were compared with the result of

frequencies of only extensional deformation. The results of the critical frequencies showed that the result of the coupled frequencies have lower results than the one with extensional theory, and concluded by stating that the torsional behavior of wires needs more study, considering the importance of such structures. To the author's knowledge, this is the only analytical study that has been done to examine the dynamic behavior due to a coupled action.

2.4 Significance of this Research

In this work, a three-dimensional, finite-element model will be applied to the double layer new trapezoidal wire, including the Poisson effect to the global axial stiffness, which has not been found before and includes the effect of varying the lay angle between 5° and 30°. Using the same approach, the global axial stiffness also will be computed for the simple straight wire rope with the same lay angles studied, thereby validating the approach in comparison with 7 different existing analytical models for this wire. For both wires the coupling action will be studied with a lay angle existing in the model. After that, free vibration using one-dimensional approximation will be performed to see the effect of such coupled stiffness behavior on the national frequencies and the normal mode where the vibration motion can be captured.

CHAPTER 3: METHOD

3.1 Overview

In this chapter, a description to what have been done to obtain the result of this research. Starts with introduction to the method used in the analysis. The approach used to predict the mechanical response of the new trapezoidal wire studied; geometry, material, and how it was analyzed and to examine the methodology and the codes used in this analysis, a well-known wire mechanical behavior, simple straight wire rope (1+6 wire) was analyzed and then compared with 7 existing analytical models available in the literature for this wire. The dynamical analysis including natural frequencies and modes shapes for an Aluminum bar modes used as a base model, then for the trapezoidal wire and the simple straight wire rope.

3.2 Finite Element Method

Converting a large problem to simple, easy, small pieces is the main characteristic of the finite element method or analysis. It is an effective method based on a numerical analysis that can solve any problem in structural mechanics, fluid flow, heat transfer, and more. The finite element method has clear steps that leads to an accurate final solution and it is powerful enough that it can deal with a very complex geometry, with isotropic or orthotropic materials. In this method, a clear picture of what is going on at any point into the system analyzed can be done easily.

3.2.1 Three-Dimensional Finite Element Method for Solving Wire's Stiffness

This section will describe in detail all the finite element analysis steps to find the mechanical behavior in the form of a 2×2 stiffness matrix for a trapezoidal wire and a simple straight strand, starting with showing the geometry and discretizing the full domain into finite elements, building the element matrices, assembling the global stiffness matrix, imposing

boundary conditions, and solving the equation (1.1) for the linear system to have the 2×2 stiffness matrix for both wires.

3.2.1.1 Discretization

In general, three-dimensional finite elements have three known solid geometry system elements that can be used: tetrahedron, wedge, and hexahedron that have 4, 6, and 8 corners (nodes), respectively. In this research, linear plane elasticity elements as hexahedron solids were used in the finite elements analysis to find the mechanical behavior of the new trapezoidal wire and the simple straight wire (1+6). Each node in the hexahedron element has three degrees of freedom in X, Y, and Z direction as displacement (u), (v), and (w), respectively. The accuracy of result is related to the number of elements discretized, to be more accurate more elements is essential, and deciding that depends on the computational cost. AutoCAD was used to discretize both wires to make sure that the x, y, and z coordinates of each node are very accurate.

3.2.1.1.1 Trapezoidal Wire

The wire has two layers; the outer wire layer has 14 aluminum wires, and the inner wire layer has 8 aluminum wires with a trapezoidal cross section wound around a carbon/glass fiber polymer composite core with a circular section (Figure 1.1). At first, the x and y plan of the back face of the wire was plot in AutoCAD. As can be seen in Figure 3.1, the gray color shows the aluminum material elements, the yellow shows the glass fiber polymer material elements, the black shows the carbon fiber polymer material elements, and the red shows the slip material elements or the gaps between the layers and the wires, which has been included in the analysis to give more accurate results.

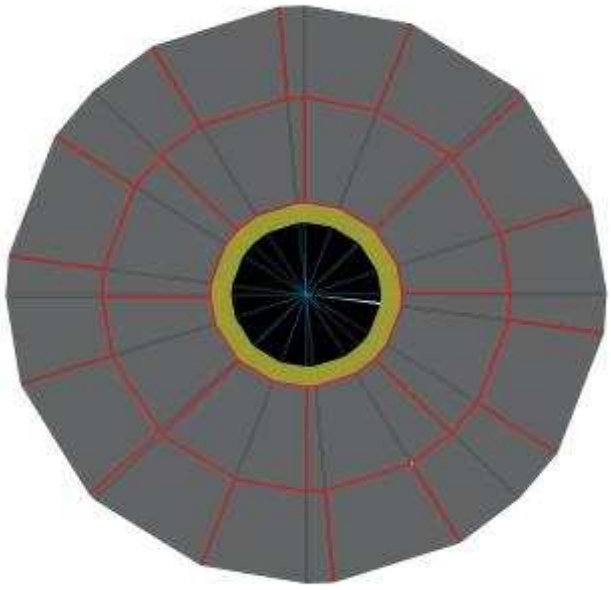

Figure 3.1 The new trapezoidal wire's x and y plan on the back face.

Then, each node on this face was given a number from 1 to 265, the total number of nodes in the back face being 265. With an arbitrary length, the front face was also plotted and the nodes were numbered from 266 to 530. The total number of nodes in the system is 530. Then, each node on the back face was connected to its corresponding node on the front face, after numbering the system elements from 1 to 264. Each element has a trapezoidal solid with 8 nodes (Figure 3.2). In addition, each node has 3 degrees of freedom in x as (u) displacement, y as (v) displacement, and z as (w) displacement, so, in total the system has 1,590 degrees of freedom, and each node is linked with its 3 degrees of freedom actual number, so it will be easy to apply the boundary conditions later.

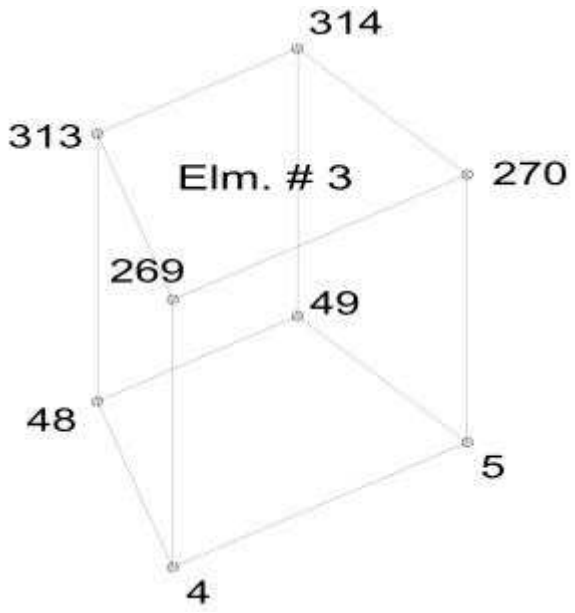

Figure 3.2 An example of the 8-nodal solid used for the finite element analysis.

The x and y local coordinates for the back face were read using an AutoCAD command and were saved to use as base coordinates. It should be noted that both the back and front face nodes have the same x and y coordinates with different z coordinate values at this point, which indicates that the wire is now straight with no twist. The connectivity array was computed manually and, for example, for element number 3 in Figure 3.2 the connectivity array is 4,5,270,269,48,49,314,313.

In this work, all the wire layers have a single helix around the center wire, the helix radius R_h was assumed to be 7 mm, which is the length from the center point to the middle of the inner wires and the half radius if the sections were assumed to be circular (14 mm).

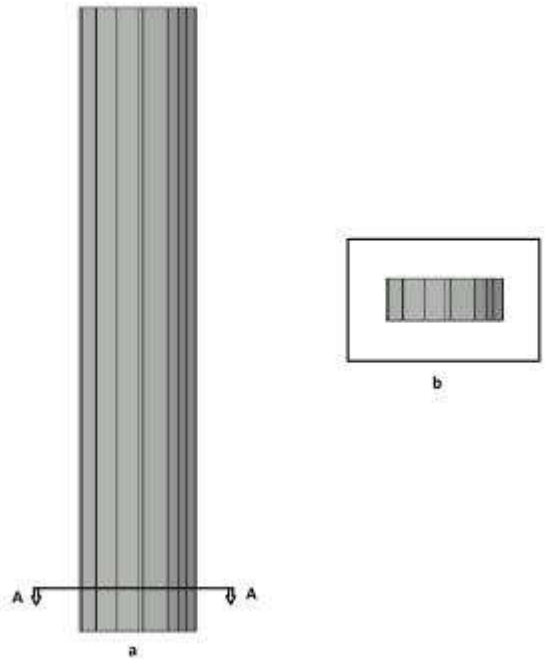

Figure 3.3.a,b Trapezoidal wire with 0 degrees lay angle.

Lay or pitch length denoted as p is the length it takes a wire to go a single round around the center core, modeling this will yield an inaccurate result because of the curve lines from the helix. Figure 3.3.a shows the whole trapezoidal wire length with no twist. Only small individual element lengths of the wire's pitch length will be modeled to meet the required accuracy approximation Figure 3.3.b. The pitch length was first computed using equation (3.1) for the known lay angles α (0°, 5°, 10°, 15°, 20°, 25°, and 30°) and the result will be used to determine the rotation and translation of the model's front face when it will be cut for small sections; Table 3.1 shows the pitch lengths.

$$p = \frac{2\pi R_h}{\tan \alpha} \qquad (3.1)$$

Table 3.1 Pitch lengths for lay angles α : 5°, 10°, 15°, 20°, 25°, and 30° for the trapezoidal wire

Lay Angles α (°)	Pitch Length p (mm)
5	502.72
10	249.43
15	164.14
20	120.84
25	94.32
30	76.17

As indicated, for all the lay angles tested; all lay lengths (along the z axis) were discrete by length elements $L_E = 7.866\ mm$; this length was chosen as it will always be approximately less than 10% of the lay length, and the reason for using one length for all models is ease of computation and comprising between models behavior later. However, once the lay is cut at a certain length, the front face coordinates (i.e., how this face rotated around its center) become unknown; to overcome this problem the transformation angle Θ_r (in degrees) can be found using equation (3.2). Table 3.2 shows the transformation angles associated with each model.

$$\Theta_r = \frac{360^\circ}{(\frac{p}{L_E})} \qquad (3.2)$$

Table 3.2 Transformation angles Θ_r associated with each model in the trapezoidal wire

Models	Transformation Angle Θ_r
5° Lay	5.63°
10° Lay	11.35°
15° Lay	17.25°
20° Lay	23.43°
25° Lay	30.02°
30° Lay	37.17°

After the transformation angle is obtained, the front face node coordinates for each model can be calculated using the Cartesian coordinate system in equation (3.3).

$$\begin{Bmatrix} x' \\ y' \\ z' \end{Bmatrix} = \begin{bmatrix} \cos(\Theta_r) & -\sin(\Theta_r) & 0 \\ \sin(\Theta_r) & \cos(\Theta_r) & 0 \\ 0 & 0 & 1 \end{bmatrix} \begin{Bmatrix} x \\ y \\ z \end{Bmatrix} \qquad (3.3)$$

For the example of element number 3, it can be seen in Figure 3.4 that nodes 269, 270, 313, and 314 in the front face have transformed from their original coordinates at lay angle 0° to a new coordinate with 15° lay angle, for instance, by rotation value around point o, which is the center node in the front face.

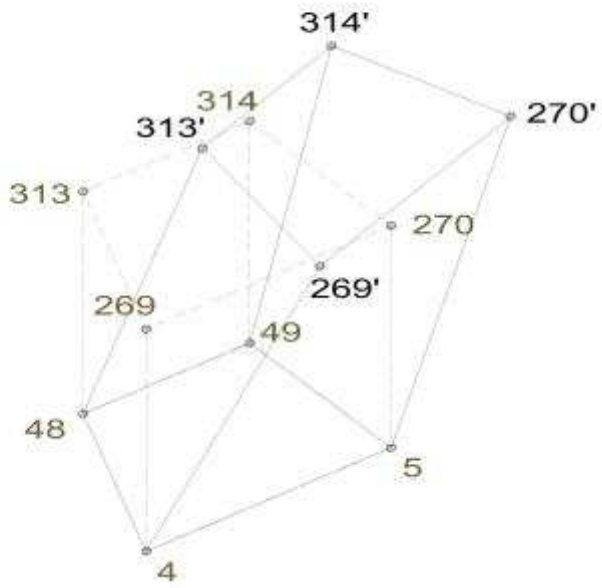

Figure 3.4 Element number 3 transformation from its original shape to the new shape.

For this work it is important to calculate the section area and the centroid for the 264 elements, for the four material properties (aluminum, glass fiber, carbon fiber, and the slip material), for many purposes, including comparing the results with one-dimensional finite element analysis for a circular bar in finding the mechanical behavior, and also when solving the vibration problem (which will be discussed later).

First, the trapezoidal area A was calculated using the closed form equation (3.4) and then the centroid Y_c was calculated in (3.5), where h is the trapezoidal element height and a and b are the base lengths. Table 3.3 shows the area of each material as well as the total area for the trapezoidal elements, when it is assumed to be a circular section with 14-mm radius.

$$A = \frac{h(a+b)}{2} \qquad (3.4)$$

$$Y_c = \frac{h(2a+b)}{3(a+b)} \qquad (3.5)$$

Table 3.3 Trapezoidal wire and circular wire section area.

Material	Area (mm^2)
Aluminum	522.21
Carbon fiber polymer	37.76
Glass fiber polymer	21.85
Slip	20.03
Total trapezoidal wire section area	601.86
Circular wire section area	615.75

3.2.1.1.2 Simple Straight Strand

This wire has one layer, which has 6 circular section metal wires, wound around a circular section core with the same material properties (Figure 1.2). A similar approach was made to conduct the x and y plan of the back face of the wire from the trapezoidal wire, taking into account the geometrical difference. However, to shorten work and analysis time for this wire, only one outer wire and the core wire were modeled and they were modeled separately, then their results were added. As can be seen in Figure 3.5, the core wire with $R_c = 1.95\ mm$ was first modeled, then the one outer wire with $R_w = 1.86\ mm$ was modeled (Figure 3.6), the total section area being $A = 77.50\ mm^2$.

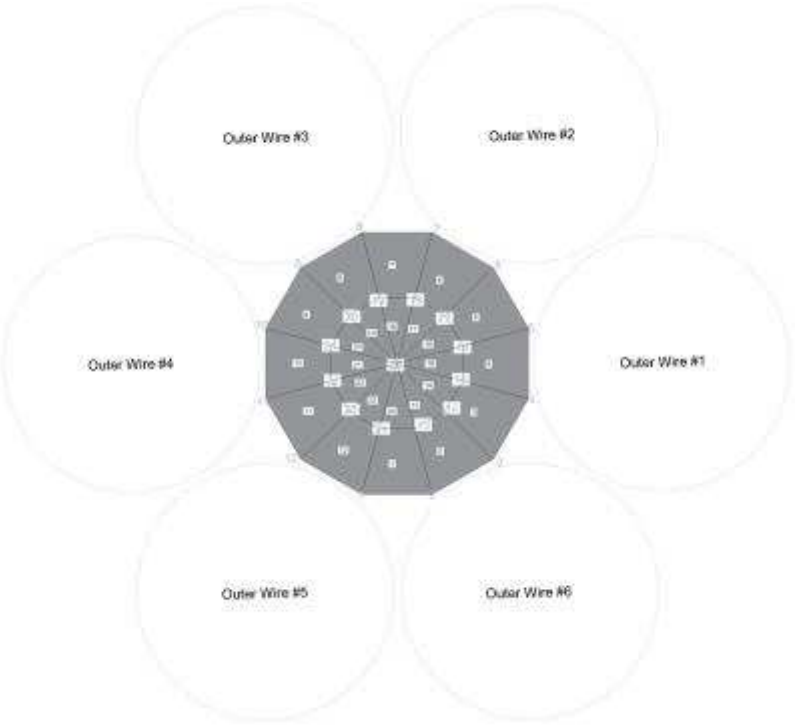

Figure 3.5 Discretization of the center core.

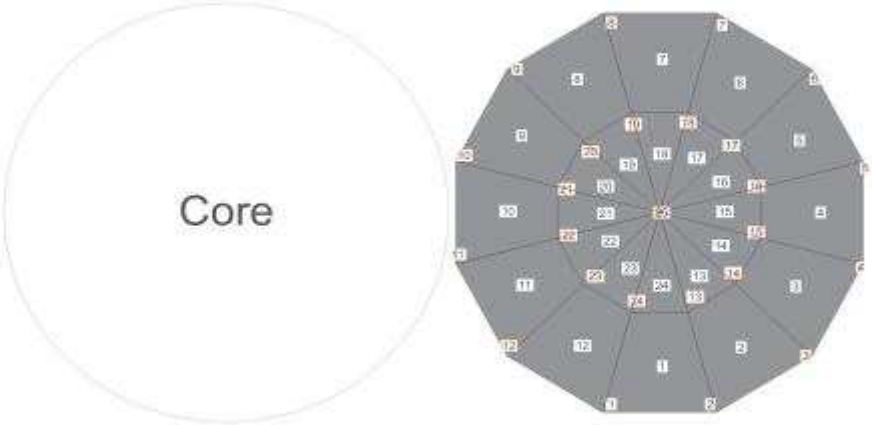

Figure 3.6 Discretization of one outer wire.

For each model, each node in this face was also given a number from 1 to 25, the total number of nodes on the back face being 25. With arbitrary length the front face was also drawn

and the nodes were numbered from 25 to 50. The total number of nodes in the wire is 50. Each node in the back face was connected to its corresponding node, and the wire was given element numbers from 1 to 24. Elements also were solid with 8 nodes (Figure 3.2). The same degrees of freedom were given for this wire x, y, and z, the system in total having 150 degrees of freedom.

The coordinates for the back face were read and saved to use as base coordinates. At this point, the back and front face nodes have the same x and y coordinates with different z coordinate values. The connectivity array was conducted in the same way as the trapezoidal wire.

For the simple straight strand, wires have a single helix around the center core wire, the helix radius R_h being calculated using equation (3.6):

$$R_h = R_c + R_w \qquad (3.6)$$

For the outer wire, as the lay angle increases the major axis R_{w2} of the circle will increase, resulting in an elliptical shape. The major axis was calculated using equation (3.7). As a result, for each of the lay angles studied, each outer model has to be revised to change the geometry and coordinates as a result of the change in the major axis. However, this change has been ignored when modeling the trapezoidal wire due to the complexity and since the change will vary the result by 1% to 2%, which was been tested on the simple straight strand.

$$R_{w2} = \frac{R_h}{\cos \alpha} \qquad (3.7)$$

As in the trapezoidal wire, only small individual element lengths of the wire's pitch length (Table 3.4) will be modeled to meet the required accuracy approximation for the known lay angles α (0°, 5°, 10°, 15°, 20°, 25°, and 30°) and the result will be used to determine the rotation and translation of the model's front face when cut for a small section.

Table 3.4 Pitch lengths for lay angles αu: 5°, 10°, 15°, 20°, 25°, and 30° for the simple straight strand.

Lay Angles α (°)	Pitch Length p (mm)
5	275.41
10	136.65
15	89.92
20	66.20
25	51.67
30	41.73

The same z axis discretization length element $L_E = 7.866\, mm$ is used for the simple strand, and the transformation angle Θ_r (in degrees) is also calculated using equation (3.2). Table 3.5 shows the transformation angles associated with each model.

Table 3.5 Transformation angles Θr associated with each model in the simple straight strand.

Models	Transformation Angle Θ_r
5° Lay	10.28°
10° Lay	20.72°
15° Lay	31.48°
20° Lay	42.77°
25° Lay	54.80°
30° Lay	67.84°

After calculating the transformation angle, the front face nodes coordinates were found using the Cartesians coordinate system in equation (3.3).

3.2.1.2 Building the Element Matrices

The governing equation is a differential equation of equilibrium in the Cartesian coordinate system for a hexahedron shape for the three types of plan elasticity, which can be expressed in expanded form and indicial form as:

$$\frac{\partial \sigma_{xx}}{\partial x} + \frac{\partial \sigma_{yx}}{\partial y} + \frac{\partial \sigma_{zx}}{\partial z} + f_x = 0$$

$$\frac{\partial \sigma_{xy}}{\partial x} + \frac{\partial \sigma_{yy}}{\partial y} + \frac{\partial \sigma_{zy}}{\partial z} + f_y = 0$$

$$\frac{\partial \sigma_{xz}}{\partial x} + \frac{\partial \sigma_{yz}}{\partial y} + \frac{\partial \sigma_{zz}}{\partial z} + f_z = 0$$

Or, $$\sigma_{ij,j} + f_i = 0 \qquad (3.8)$$

(where $\sigma_{ij,j}$ is the stress component, and f_i is the body force in x, y, and z directions).

Assuming small displacement, the strain displacement relations are represented in expanded form and indicial form:

$$\varepsilon_{xx} = \frac{\partial u}{\partial x}$$

$$\varepsilon_{yy} = \frac{\partial v}{\partial y}$$

$$\varepsilon_{zz} = \frac{\partial w}{\partial z}$$

$$\varepsilon_{xy} = \frac{1}{2}\left(\frac{\partial u}{\partial y} + \frac{\partial v}{\partial x}\right)$$

$$\varepsilon_{xz} = \frac{1}{2}\left(\frac{\partial u}{\partial z} + \frac{\partial w}{\partial x}\right)$$

$$\varepsilon_{yz} = \frac{1}{2}\left(\frac{\partial v}{\partial z} + \frac{\partial w}{\partial y}\right)$$

Or, $$\varepsilon_{ij} = \frac{1}{2}(u_{i,j} + u_{j,i}) \qquad (3.9)$$

(where ε_{ij} is the linear strain component in xx, yy, and zz plan and the engineering shear strain component in xy, xz, and yz plan).

Stress strain or constitutive relations is expressed by generalized Hook's law of elastic stiffness tensor C_{ijkl} in equation (3.10):

$$\sigma_{ij} = C_{ijkl}\varepsilon_{kl} \qquad (3.10)$$

To calculate the elastic stiffness constant C_{ijkl}, the elastic compliance constant S_{ijkl} was computed in (3.11) for each material in the trapezoidal wire and the simple straight strand. Note that the elastic stiffness constant is the inverse of the elastic compliance constant in matrix form.

$$S_{ijkl} = \begin{bmatrix} \frac{1}{E} & \frac{-v}{E} & \frac{-v}{E} & 0 & 0 & 0 \\ \frac{-v}{E} & \frac{1}{E} & \frac{-v}{E} & 0 & 0 & 0 \\ \frac{-v}{E} & \frac{-v}{E} & \frac{1}{E} & 0 & 0 & 0 \\ 0 & 0 & 0 & \frac{1}{G} & 0 & 0 \\ 0 & 0 & 0 & 0 & \frac{1}{G} & 0 \\ 0 & 0 & 0 & 0 & 0 & \frac{1}{G} \end{bmatrix} \qquad (3.11)$$

In Table 3.6, which details the engineering constant (elastic modulus E, Poisson ratio υ, shear modulus G, and density ρ) for the trapezoidal wire, note that the slip's properties have been assumed to be 0.0001% of the aluminum's properties. And, for the simple straight strand the engineering constant used are exact same material found and used in the analytical and experimental literature were $\mathrm{E} = 197.9\ \mathrm{GPa}$, $\upsilon = 0.3$, $\mathrm{G} = 76.11\ \mathrm{GPa}$, and $\rho = 7700\ \frac{\mathrm{kg}}{\mathrm{m}^3}$.

Table 3.6 The engineering constant for trapezoidal wire.

	Aluminum	Carbon Fiber	Glass Fiber
Elastic modulus E (GPa)	69	230	76
Poisson ratio υ	0.33	0.30	0.22
Shear modulus G (GPa)	25.94	88.46	31.15
Density ρ ($\frac{\text{kg}}{\text{m}^3}$)	2710	1800	2580

To find the weak form, the three governing differential equations (3.8) will be multiplied by a weight function, w_1, w_2, and w_3, respectively, then integrated by parts, so we have:

$$\int_{\Omega^e} w_1[\frac{\partial \sigma_{xx}}{\partial x} + \frac{\partial \sigma_{yx}}{\partial y} + \frac{\partial \sigma_{zx}}{\partial z} + f_x]dxdydz = 0 \qquad (3.12)$$

$$\int_{\Omega^e} w_2[\frac{\partial \sigma_{xy}}{\partial x} + \frac{\partial \sigma_{yy}}{\partial y} + \frac{\partial \sigma_{zy}}{\partial z} + f_y]dxdydz = 0 \qquad (3.13)$$

$$\int_{\Omega^e} w_3[\frac{\partial \sigma_{xz}}{\partial x} + \frac{\partial \sigma_{yz}}{\partial y} + \frac{\partial \sigma_{zz}}{\partial z} + f_z]dxdydz = 0 \qquad (3.14)$$

So, it will be:

$$0 = \int_{\Omega^e}[\frac{-\partial w_1}{\partial x}(C_{11}\frac{\partial u}{\partial x} + C_{12}\frac{\partial v}{\partial y} + C_{13}\frac{\partial w}{\partial z}) - \frac{\partial w_1}{\partial y}\left(\frac{1}{2}C_{66}\left(\frac{\partial u}{\partial y} + \frac{\partial v}{\partial x}\right)\right) - \frac{\partial w_1}{\partial z}\left(\frac{1}{2}C_{55}\left(\frac{\partial u}{\partial z} + \frac{\partial w}{\partial x}\right)\right) + w_1 f_x]dxdydz \qquad (3.15)$$

$$0 = \int_{\Omega^e}[\frac{-\partial w_2}{\partial x}(\frac{1}{2}C_{66}\left(\frac{\partial u}{\partial y} + \frac{\partial v}{\partial x}\right)) - \frac{\partial w_2}{\partial y}(C_{21}\frac{\partial u}{\partial x} + C_{22}\frac{\partial v}{\partial y} + C_{23}\frac{\partial w}{\partial z}) - \frac{\partial w_2}{\partial z}(\frac{1}{2}C_{44}\left(\frac{\partial v}{\partial z} + \frac{\partial w}{\partial y}\right)) + w_2 f_y]dxdydz \qquad (3.16)$$

$$0 = \int_{\Omega^e}[\frac{-\partial w_3}{\partial x}(\frac{1}{2}C_{55}\left(\frac{\partial u}{\partial z}+\frac{\partial w}{\partial x}\right)) - \frac{\partial w_3}{\partial y}\left(\frac{1}{2}C_{44}\left(\frac{\partial v}{\partial z}+\frac{\partial w}{\partial y}\right) - \frac{\partial w_3}{\partial z}\left(C_{13}\frac{\partial u}{\partial x}+C_{23}\frac{\partial v}{\partial y}+ C_{33}\frac{\partial w}{\partial z}\right)\right) + w_3 f_z]dxdydz \quad (3.17)$$

The finite element approximation can be written as:

$$u(x,y,z) = \sum_{j=1}^{n} u_j \psi_j^u(x,y,z) \quad (3.18)$$

$$v(x,y,z) = \sum_{j=1}^{n} v_j \psi_j^v(x,y,z) \quad (3.19)$$

$$w(x,y,z) = \sum_{j=1}^{n} v_j \psi_j^w(x,y,z) \quad (3.20)$$

And:

$$w_1 = \psi_i^u(x,y,z) \quad (3.21)$$

$$w_2 = \psi_i^v(x,y,z) \quad (3.22)$$

$$w_3 = \psi_i^w(x,y,z) \quad (3.23)$$

After that, for the 8-nodal element, each node has three degrees of freedom, so the element matrix will be 24×24 of:

$$\begin{bmatrix} [K^{11}] & [K^{12}] & [K^{13}] \\ [K^{21}] & [K^{22}] & [K^{23}] \\ [K^{31}] & [K^{32}] & [K^{33}] \end{bmatrix} \begin{Bmatrix} \{u\} \\ \{v\} \\ \{w\} \end{Bmatrix} = \begin{Bmatrix} \{f^1\} \\ \{f^2\} \\ \{f^3\} \end{Bmatrix} \quad (3.24)$$

Then the matrices for the 264-element trapezoidal wire and the 24-element simple straight strand can be assembled.

3.2.1.3 Imposing the Boundary Conditions

In order to find the overall mechanical behavior of the trapezoidal wire and the simple straight strand represented in the stiffness coefficients in equation (1.1), the boundary conditions have two cases, defined as follows: first, at one end (the back face), all node-essential boundary conditions: displacement (u) in x direction, displacement (v) in y direction, and displacement (w)

in z direction were prescribed to be zero, meaning this face is fully clamped. The other end (front face) nodes, having a value of one (a unit displacement) in axial displacement (w) in z direction, displacement (u) in x axis, and displacement (v) in y axis, were set to be zero. Similarly, for the back face, all node displacements are set to be zero; however, the other face (front face) displacements in x and y were having an equivalent amount of value to present a unit rotation, and the displacement (w) in z direction was set to be zero. For example, node 4 and its corresponding node 269 in element number 3 in Figure 3.2 will have, in the first case, node 4 (u=0, v=0, and w=0) and node 269 (u=0, v=0, w=1), and, for the second case, node 4 (u=0, v=0, and w=0) and node 269 (u=0.0117, v=0.0064, and w=0).

3.2.1.4 Solving the Global Stiffness Matrix

After inserting all the above in the input file to be solved using a Fortran 77 code, the code was run two times for the seven different lay angle models for each wire, the trapezoidal wire and the simple straight strand, the result is represented as forces in x, y, and z direction of the front face. To solve the stiffness coefficients by applying the equations of equilibrium, two steps were followed: the total forces in z direction F_z comprise the pure tensile stiffness $k_{\varepsilon\varepsilon}$, the coupled stiffness between tensile and the torsional term $k_{\varepsilon\theta}$ is the forces in x and in y direction multiplied by the length from the origin to node, which is the moment around the z direction M_z, and that is the solution from applying the first boundary condition meaning these coefficients are the forces required to hold one unit displacement. As for applying the second boundary condition, the forces required to hold one unit rotation, coupled stiffness between tensile and the torsional term $k_{\theta\varepsilon}$ is the total forces in z direction F_z, and torsional stiffness $k_{\theta\theta}$ is the moment around the z direction M_z for this case. In the end, 14 stiffness matrices were computed, for both the trapezoidal

aluminum wire and the simple straight strand for all lay angles α: 0°, 5°, 10°, 15°, 20°, 25°, and 30°.

3.3 Analytical Models

For the simple straight strand (1+6) there are many mathematical models, depending on different theories. In this work, to validate the finite element approach, 7 of the analytical models presented in the literature were chosen here, namely, the Hruska, McConnell and Zemek**,** Machida and Durelli**,** Knapp**,** Kumar and Cochran**,** Sathikh, and Labrosse models. A general idea and the closed form equations to find the stiffness coefficients are presented for each model. All the results from these models were then compared with the finite element model used in this research. Most of these equation are replicated from Ghoreishi, Messager, et al. (2007).

3.3.1 Hruska's Model

As described, this model is the simplest; it only accounted for axial tension and ignored the torsion and bending. The stiffness coefficients can be found using:

$$k_{\varepsilon\varepsilon} = AE_c + 6AE_w \cos(\alpha)^3$$

$$k_{\varepsilon\theta} = 6AE_w R_h \cos(\alpha)^2 \sin(\alpha)$$

$$k_{\theta\varepsilon} = 6AE_w R_h \cos(\alpha)^2 \sin(\alpha)$$

$$k_{\theta\theta} = GJ_c + 6AE_w R_h^2 \cos(\alpha) \sin(\alpha)^2 \qquad (3.25)$$

(where AE represents the axial stiffness and GJ represents the torsional stiffness, while subscripts c and w are related to core and wire properties).

3.3.2 McConnell and Zemek's Model

This model simply modified Hurska's model by including the total stiffness torsion of the 6 wires in stiffness torsion term equation $k_{\theta\theta}$, the rest remaining unchanged:

$$k_{\varepsilon\varepsilon} = AE_c + 6AE_w \cos(\alpha)^3$$

$$k_{\varepsilon\theta} = 6AE_w R_h \cos(\alpha)^2 \sin(\alpha)$$

$$k_{\theta\varepsilon} = 6AE_w R_h \cos(\alpha)^2 \sin(\alpha)$$

$$k_{\theta\theta} = GJ_c + 6GJ_w + 6AE_w R_h^2 \cos(\alpha) \sin(\alpha)^2 \qquad (3.26)$$

3.3.3 Machida and Durelli's Model

This model added the bending and torsion stiffness to the global stiffness matrix; however, $k_{\varepsilon\varepsilon}$ and $k_{\varepsilon\theta}$ remain unchanged:

$$k_{\varepsilon\varepsilon} = AE_c + 6AE_w \cos(\alpha)^3$$

$$k_{\varepsilon\theta} = 6AE_w R_h \cos(\alpha)^2 \sin(\alpha)$$

$$k_{\theta\varepsilon} = 6(AE_w R_h \cos(\alpha)^2 \sin(\alpha) - \frac{2EI_w}{R_h} \cos(\alpha)^2 \sin(\alpha)^3$$

$$+ \frac{GJ_w}{R_h} \cos(\alpha)^2 \sin(\alpha)\,(1 - 2\cos(\alpha)^2))$$

$$k_{\theta\theta} = GJ_c + 6(AE_w R_h^2 \cos(\alpha) \sin(\alpha)^2 + 2EI_w \cos(\alpha)^3 \sin(\alpha)^2 + GJ_w \cos(\alpha)^3\,(1 -$$

$$2\sin(\alpha)^2)) \qquad (3.27)$$

Here, EI represent the bending stiffness.

3.3.4 Knapp's Model

This model focused on the compressibility of the steel core, which is the change in the core radius due to pressure; the equation then can be written as:

$$k_{\varepsilon\varepsilon} = AE_c + 6AE_w \cos(\alpha\zeta)^3$$

$$k_{\varepsilon\theta} = 6AE_w R_h \cos(\alpha\eta)^2 \sin(\alpha)$$

$$k_{\theta\varepsilon} = 6(AE_w R_h \sin(\alpha\zeta) - \frac{EI_w}{R_h}(\lambda + 2\zeta)(\frac{GJ_w}{R_h}(1 - 2\zeta)\cos(\alpha)^2 \sin(\alpha)))$$

$$k_{\theta\theta} = GJ_c + 6(AE_w R_h \eta \sin(\alpha) - \frac{EI_w}{R_h}(\mu + 2\eta - \frac{2R_h}{\tan(\alpha)}) \sin(\alpha)^3 +$$

$$\frac{GJ_w}{R_h}\left(\frac{R_h}{\tan(\alpha)} - 2\mu\right) \cos(\alpha)^2 \sin(\alpha)) \qquad (3.28)$$

ζ, η, λ, and μ are geometric and elastic properties; and for a steel core:

$$\zeta = \cos(\alpha)^2$$

$$\eta = R_h \sin(\alpha)\cos(\alpha)$$

$$\lambda = \mu = 0 \qquad (3.29)$$

3.3.5 Kumar and Cochran's Model

This model linearized Costello's model and included the Possion ratio:

$$k_{\varepsilon\varepsilon} = AE_c + 6AE_w \cos(\alpha)\,(1 - (1 + \nu)\,\mathrm{p}\,\sin(\alpha)^2$$

$$k_{\varepsilon\theta} = 6AE_w R_h\,\mathrm{p}\,\cos(\alpha)^2\,\sin(\alpha)$$

$$k_{\theta\varepsilon} = 6(AE_w R_h \sin(\alpha) - \frac{EI_w}{R_h}\,\sin(\alpha)\,(1 - \nu_f\,\cos(\alpha)^4 + (1 + \nu)\big(q - 1 + \nu_f \cos(\alpha)^4\big))$$

$$k_{\theta\theta} = GJ_c + 6EI_w q\,\cos(\alpha) \qquad (3.30)$$

p, q, ν_1, and ν_f are:

$$p = (1 - \nu_1)(1 - \frac{1}{4}\left(\frac{R_w}{R_h}\right)^2 (1 + \nu_f \cos(2\alpha))\,\sin(\alpha)^2) \qquad (3.31)$$

$$q = (1 - \nu_1)(\frac{1}{4}\left(\frac{R_w}{R_h}\right)^2 \sin(\alpha)^2 + 1 - \sin(\alpha)^4 - \nu_f \cos(\alpha)^4 \cos(2\alpha)) \qquad (3.32)$$

$$\nu_1 = \nu\frac{R_w}{R_h}\sin(\alpha)^2 \qquad (3.33)$$

$$\nu_f = \frac{\nu}{(1+\nu)} \qquad (3.34)$$

3.3.6 Sathikh's Model

Most of the early models have lack of symmetry when the torsion and bending is included, so this model is a driven, closed-form, symmetric linear elastic equation:

$$k_{\varepsilon\varepsilon} = AE_c + 6(AE_w \cos(\alpha)^3 + (GJ_w \sin(\alpha)^2 + EI_w \cos(\alpha)^2)\frac{\sin(\alpha)^4 \cos(\alpha)}{R_h^2})$$

$$k_{\varepsilon\theta} = 6(AE_w R_h \cos(\alpha)^2 \sin(\alpha) + (GJ_w \cos(\alpha)^2 - EI_w(1 + \cos(\alpha)^2))\frac{\sin(\alpha)^4 \cos(\alpha)}{R_h^2})$$

$$k_{\theta\varepsilon} = 6(AE_w R_h \cos(\alpha)^2 \sin(\alpha) + (GJ_w \cos(\alpha)^2 - EI_w(1 + \cos(\alpha)^2))\frac{\sin(\alpha)^4 \cos(\alpha)}{R_h^2})$$

$$k_{\theta\theta} = GJ_c + 6(AE_w R_h^2 \cos(\alpha) \sin(\alpha)^2 + GJ_w \cos(\alpha)^7 + EI_w \sin(\alpha)^2 \cos(\alpha)\ (1 + \cos(\alpha)^2)^2)$$

(3.35)

3.3.7 Labrosse's Model

This model included the bending and the torsion, so the stiffness components will be:

$$k_{\varepsilon\varepsilon} = AE_c + 6AE_w \cos(\alpha)^3$$

$$k_{\varepsilon\theta} = 6AE_w R_h \cos(\alpha)^2 \sin(\alpha)$$

$$k_{\theta\varepsilon} = 6AE_w R_h \cos(\alpha)^2 \sin(\alpha)$$

$$k_{\theta\theta} = GJ_c + 6(AE_w R_h^2 \cos(\alpha) \sin(\alpha)^2 + GJ_w \cos(\alpha)^5 + EI_w \sin(\alpha)^2 \cos(\alpha)\ (1 + \cos(\alpha)^2))$$

(3.36)

3.3 Free Vibration Analysis

For the trapezoidal wire and the simple straight strand, a free vibration analysis was applied, assuming tight wire (fixed-fixed) at both ends with no sag for one-dimensional approximation. A Matlab code was used to solve for the eigenvalues which are the natural frequencies and the eigenvectors as the normal mode shapes. To check the approach used and the code, the straight 14-mm radius of a circular aluminum bar was discretized along its length and analyzed; this bar had a 2.3% different area section from that of the trapezoidal wire, and the results of this bar will be compared with a one-dimensional known exact solution.

3.3.1 Aluminum Circular Bar

The governing equation based on simple harmonic motion for the free vibration of undamped two degrees of freedom is given as:

$$(-\omega^2[M] + [K])\begin{Bmatrix} u \\ \theta \end{Bmatrix} = 0 \qquad (3.37)$$

$$u(x,t) = U(x)\sin\omega t \qquad (3.38)$$

$$\theta(x,t) = \theta(x)\sin\omega t \qquad (3.39)$$

(where ω is the natural frequency, M the mass matrix assembled for one-dimensional approximation, K is the stiffness matrix assembled for one-dimensional approximation, u is the global axial displacement, and θ is the global twist angle).

First, that global mass matrix which is the kinetic energy of the section has to be computed, and for the two degrees of freedom (axial and twist), as a result a 2×2 matrix has to be found for each section studied:

$$m_{ij} = \begin{bmatrix} m_{\varepsilon\varepsilon} & m_{\varepsilon\theta} \\ m_{\theta\varepsilon} & m_{\theta\theta} \end{bmatrix} \qquad (3.40)$$

(where $m_{\varepsilon\varepsilon}$ is the axial mass, $m_{\theta\varepsilon}$ and $m_{\varepsilon\theta}$ are the coupling mass between axial and twist, and $m_{\theta\theta}$ is the torsional mass term). It should be known that there is no coupling mass between axial and twist ($m_{\theta\varepsilon} = m_{\varepsilon\theta} = 0$).

The axial mass $m_{\varepsilon\varepsilon}$ can be found from approximating the axial displacement and integrating the mass over that particular domain, which means basically integrating the mass over the area. Where the density is a constant will be multiplied by the area in closed form, for the circular aluminum bar:

$$m_{\varepsilon\varepsilon} = \rho_{Al} \times A_{circle} \qquad (3.41)$$

(where ρ_{Al} is the aluminum density and A_{circle} is the section area of the circular bar).

Then, the torsional mass $m_{\theta\theta}$ can be found by multiplying the torsional stiffness by the density of that particular element in closed form. In the aluminum bar case:

$$m_{\theta\theta} = \rho_{Al} \times J_{circle} = \rho_{Al}(\frac{\pi}{2}r) \qquad (3.42)$$

(where J is the torsional stiffness and r is the radius).

After solving the global matrix equation (3.40), this matrix has to be discretized to one-dimensional approximation over length; with the two degrees of freedom (axial and twist), the mass matrix is a 4×4 can be written as:

$$m_{ij} = \begin{bmatrix} \frac{m_{\varepsilon\varepsilon}L}{3} & 0 & \frac{m_{\varepsilon\varepsilon}L}{6} & 0 \\ 0 & \frac{m_{\vartheta\vartheta}L}{3} & 0 & \frac{m_{\vartheta\vartheta}L}{6} \\ \frac{m_{\varepsilon\varepsilon}L}{6} & 0 & \frac{m_{\varepsilon\varepsilon}L}{3} & 0 \\ 0 & \frac{m_{\vartheta\vartheta}L}{6} & 0 & \frac{m_{\vartheta\vartheta}L}{3} \end{bmatrix} \qquad (3.43)$$

Second, the global stiffness matrix (which was discussed in section 3.2 of this chapter) has to be found. However, for the aluminum bar, pure tensile stiffness $k_{\varepsilon\varepsilon}$is represented by $(E_{Al}A_{circle})$, where E_{Al} is the modulus of elasticity for aluminum (the constant can be found in Table 3.6), with no coupling stiffness terms between the tensile and the torsional, since the bar is straight ($k_{\varepsilon\theta} = k_{\theta\varepsilon} = 0$), and the global torsional stiffness $k_{\theta\theta}$ is represented by $(G_{Al}J_{circle})$, where G_{Al} is the shear modulus from Table 3.6.

Similarly, after the global stiffness matrices are obtained, it has to be discretized to find the one-dimensional approximation over a specific length, and since two degrees of freedom (axial and twist) is assumed, the stiffness matrix is a 4×4:

$$k_{ij} = \begin{bmatrix} \frac{k_{\varepsilon\varepsilon}}{h} & \frac{k_{\varepsilon\vartheta}}{h} & -\frac{k_{\varepsilon\varepsilon}}{h} & -\frac{k_{\varepsilon\vartheta}}{h} \\ \frac{k_{\vartheta\varepsilon}}{h} & \frac{k_{\vartheta\vartheta}}{h} & -\frac{k_{\vartheta\varepsilon}}{h} & -\frac{k_{\vartheta\vartheta}}{h} \\ -\frac{k_{\varepsilon\varepsilon}}{h} & -\frac{k_{\varepsilon\vartheta}}{h} & \frac{k_{\varepsilon\varepsilon}}{h} & \frac{k_{\varepsilon\vartheta}}{h} \\ -\frac{k_{\varepsilon\vartheta}}{h} & -\frac{k_{\vartheta\vartheta}}{h} & \frac{k_{\vartheta\varepsilon}}{h} & \frac{k_{\vartheta\vartheta}}{h} \end{bmatrix} \qquad (3.44)$$

After finding the element mass matrix and element stiffness matrix for the aluminum bar case, a length of 8 m was discretized into 2, 4, 8, and 16 elements. Then, assembling to find the global matrix (34×34) for 16 elements for one-dimensional approximation and applying the boundary condition which is fixing both ends, the global matrix will be (30×30). The results then will be checked for convergence with the exact solution of fixed-fixed bar equations for the axial and torsional natural frequencies:

$$\omega_A = \frac{\pi}{L}\sqrt{\frac{E_{Al}}{\rho_{Al}}} \qquad (3.45)$$

$$\omega_T = \frac{\pi}{L}\sqrt{\frac{G_{Al}}{\rho_{Al}}} \qquad (3.46)$$

(where ω_A, ω_T, and L are the axial frequency, the torsional frequency, and the bar length, respectively).

3.3.2 Trapezoidal Wire

The free vibration analysis was also applied on the trapezoidal wire for all the lay angles (0°, 5°, 10°, 15°, 20°, 25°, and 30°) to observe the behavior and the changes in the natural frequencies and normal modes and study them.

Finding the global mass matrix was more complex for the trapezoidal wire, due to the different trapezoidal elements areas and shapes (Figure 3.1). For the axial mass $m_{\varepsilon\varepsilon}$ as same as the circular bar approach was used, however, three more materials had to be added:

$$m_{\varepsilon\varepsilon} = (\rho_{Al} \times A_{Al}) + (\rho_{CF} \times A_{CF}) + (\rho_{GF} \times A_{GF}) + (\rho_S \times A_S) \qquad (3.47)$$

(where ρ_{Al}, ρ_{CF}, ρ_{GF}, and ρ_S are aluminum, carbon fiber, glass fiber, and slip density, and A_{Al}, A_{CF}, A_{GF}, and A_S are aluminum, carbon fiber, glass fiber, and slip areas, respectively).

However, for the torsional mass $m_{\theta\theta}$, each element of the x,y planer had to be calculated individually by discretizing. To find that, first the area and centroid were calculated using

equations (3.4) and (3.5). From the centroid, the distance from the center of the section and the center of the element can be easily calculated r_θ.After that, the torsional stiffness J_{elm} was calculated, which is simply the area multiplied by the squared distance. In the end, J_{elm} will be multiplied by each element density ρ_{elm}:

$$m_{\theta\theta} = \rho_{elm} \times J_{elm} = \rho_{elm}({r_\theta}^2 A_{elm}) \qquad (3.48)$$

After constructing the global mass matrix (3.40), equation (3.43) also was used to find the element matrix for the trapezoidal wire. The global stiffness matrices for lay angles α: 0°, 5°, 10°, 15°, 20°, 25°, and 30° were already found in section 3.2. The equation (3.44) was also used to find the element stiffness matrix of the trapezoidal wire.

The natural frequencies and the normal modes were found for all the lay angles studied using the Matlab code for 16 elements of an arbitrary length (8 m) for the trapezoidal wire.

3.3.3 Simple Straight Strand

The natural frequencies and normal modes for the simple straight strand for all the lay angles (0°, 5°, 10°, 15°, 20°, 25°, and 30°) to study its behavior verse the trapezoidal wire.

As in the two previous sections, the global mass (3.40) was calculated for the simple strand using a combination of the circular bar and the trapezoidal wire approaches. Then, it was discretized for the one-dimensional matrix (4.43). Also, the global stiffness matrices were computed earlier for all the lay angles, and used here in the form of equation (4.44). The natural frequencies ω and the normal modes were found for the same length assumed (8 m).

CHAPTER 4: RESULTS AND DISCUSSION

4.1 Overview

In this chapter, the results of the methodology used in this work are presented, including the axial behavior of the trapezoidal wire studied and compared with the simple straight strand and its analytical models. The results of the free vibration analysis for the dynamic behavior of these wires are also presented.

4.2 Mechanical Behavior

The global stiffness matrix showing the axial mechanical behavior was solved for the new wire; the trapezoidal wire, and comparison was performed for lay angles α between 0°and 30°; to validate the method used, the simple straight strand was modeled and analyzed and compared with existing analytical formulations for the same lay angles used.

4.2.1 Trapezoidal Wire

Considering equation (1.1), which represents the final results for the elastic static tension torsion behavior of the trapezoidal wire, as the finite element model was run 7 times for 7 different lay angles α: 0°, 5°, 10°, 15°, 20°, 25°, and 30°, the final stiffness component in the form of a 2×2 matrix was obtained for each angle (results in Table 4.1).

Table 4.1 Comparison between the different lay angles matrix components for the trapezoidal wire.

	Stiffness matrix components			
Lay Angles α	$k_{\varepsilon\varepsilon}(kN)$	$k_{\varepsilon\theta}(Nm)$	$k_{\theta\varepsilon}(Nm)$	$k_{\theta\theta}(Nm^2)$
0°	6.71E+04	0.00E+00	0.00E+00	1.36E+03
5°	6.70E+04	8.48E+04	8.48E+04	1.42E+03
10°	6.67E+04	9.24E+04	9.24E+04	1.49E+03
15°	6.61E+04	9.98E+04	9.98E+04	1.57E+03
20°	6.52E+04	1.07E+05	1.07E+05	1.66E+03
25°	6.41E+04	1.14E+05	1.14E+05	1.75E+03
30°	6.25E+04	1.20E+05	1.20E+05	1.86E+03

Furthermore, the coupling terms had a small difference, and this difference can be resolved by increasing the element numbers, it can be recognized that the global coupling stiffness terms between the tensile and the torsional were set to be equal ($k_{\varepsilon\theta} = k_{\theta\varepsilon}$) by computing the average without losing the accuracy, which is done to avoid the contrast of the Maxwell Betti reciprocal theorem for linear elastic structures.

For the axial stiffness $k_{\varepsilon\varepsilon}$, it can be seen in Figure 4.1 that it is decreasing while the lay angles α are increasing. The different from between the stiffness of straightening the trapezoidal wire (0°) and starting twisting it as small an angle as 5° will result in a 0.15% change. However, the loss in tensile stiffness will be 7.36% for a 30° twist angle.

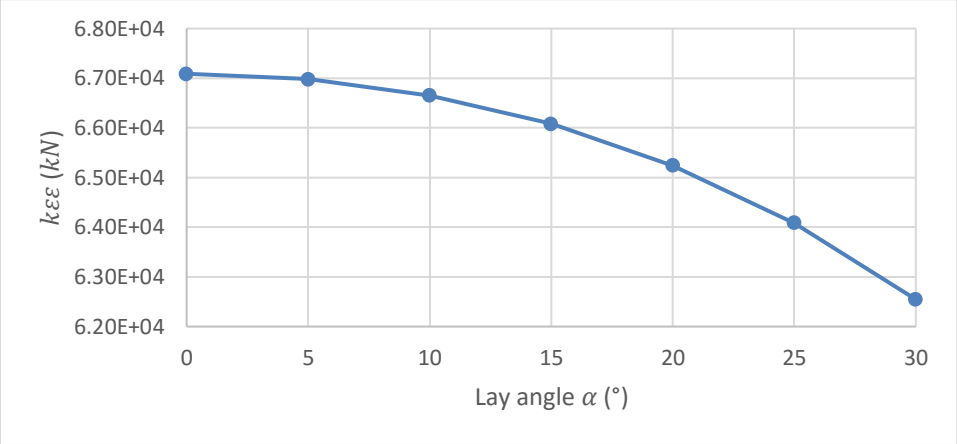

Figure 4.1 Axial stiffness $k_{\varepsilon\varepsilon}$ versus lay angles α.

The coupling coefficient terms between the tensile and the torsional $k_{\varepsilon\theta}$, and $k_{\theta\varepsilon}$ curve are linearly increasing as showing in Figure 4.2 and Figure 4.3. The results show that the coupling action will start once the wire has even a small angle twist. However, the results of a 5° twist indicate that the coupling terms will have a significant value ($84.6\ kNm$) compared to no coupling in the straight state in the trapezoidal wire.

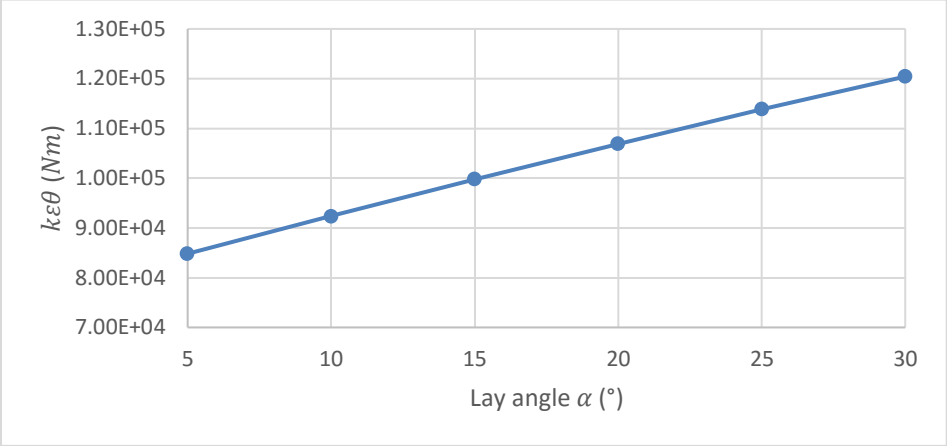

Figure 4.2 Coupling stiffness $k_{\varepsilon\theta}$ versus lay angles α.

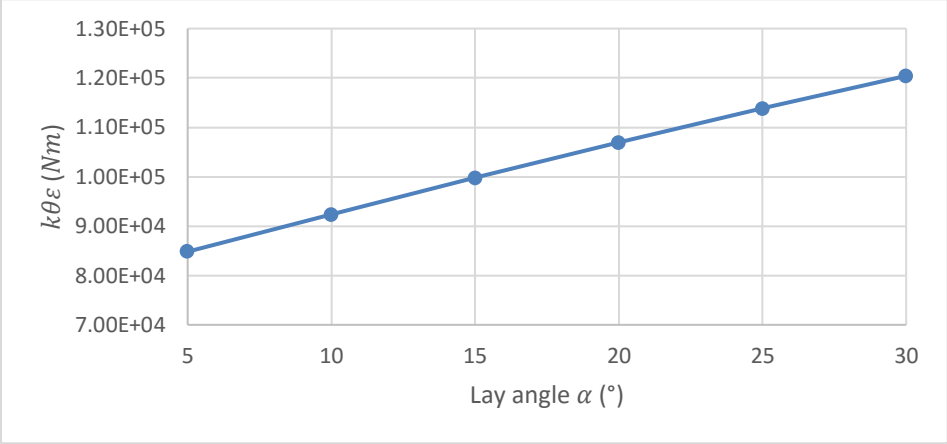

Figure 4.3 Coupling stiffness $k_{\theta\varepsilon}$versus lay angles α

The torsional stiffness $k_{\theta\theta}$ coefficients also are increasing linearly as the lay angle is increasing, as can be seen in Figure 4.4. Furthermore, the stiffness will increase 4.41% by merely increasing the twist from a 0° to a 5° angle, and a significant increase by 36.76% if twisted 30°. It can still be seen that it has a smaller contribution when it is compared with the axial stiffness $k_{\varepsilon\varepsilon}$.

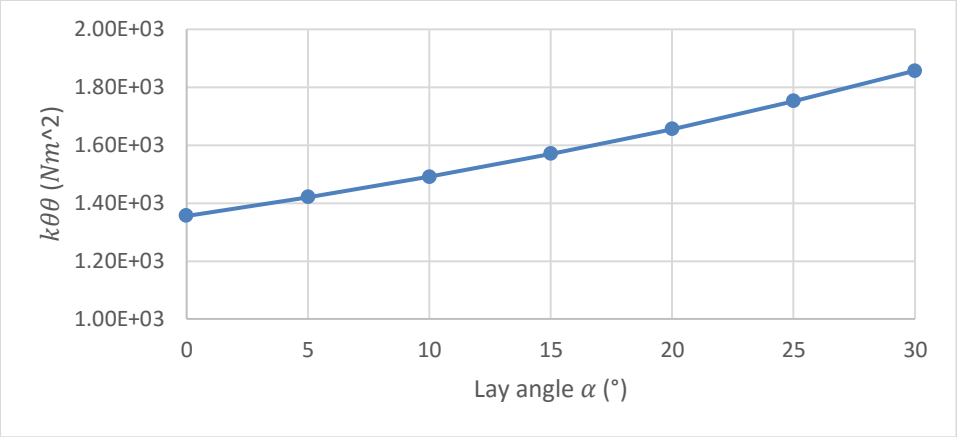

Figure 4.4 Torsional stiffness $k_{\theta\theta}$ versus lay angles α.

This new trapezoidal wire showed a great result for the most practical lay angles α between 0° and 30° compared with existing wire, of which some can have lower stiffness behavior even at 23° and higher. However, it should be noted that, for this trapezoidal wire, at some higher twisting angle, the results will start significantly deceasing for the coupling term and torsion term.

4.2.2 Simple Straight Strand

To verify the method used to solve for the mechanical behavior of the trapezoidal wire, the same approach used in the finite 24-element model for this wire was also studied by varying the twist angle used in the comparison. (The goal here is only checking that the methodology used can yield a good approximation for a wire with a large number of elements.) The four elastic stiffness components in the form of a 2×2 matrix were obtained for each lay angle α between 0° and 30° (results in Table 4.2); it can be readily seen that the results are smaller than those for the trapezoidal wire due to the simple straight strand section's small size. Then the results of the simple straight strand finite element model were compared with the seven analytical models available in the literature by Hruska, McConnell and Zemek**,** Machida and Durelli**,** Knapp, Kumar and Cochran**,** Sathikh, and Labrosse.

Table 4.2 Comparison between the different lay angles matrix components for the simple straight strand.

	Stiffness matrix components			
Lay Angles α	$k_{\varepsilon\varepsilon}(kN)$	$k_{\varepsilon\theta}(Nm)$	$k_{\theta\varepsilon}(Nm)$	$k_{\theta\theta}(Nm^2)$
0°	1.67E+04	0.00E+00	0.00E+00	3.58E+01
5°	1.66E+04	5.57E+03	5.57E+03	4.20E+01
10°	1.64E+04	7.98E+03	7.98E+03	5.07E+01
15°	1.61E+04	1.03E+04	1.03E+04	6.21E+01
20°	1.57E+04	1.26E+04	1.26E+04	7.60E+01
25°	1.51E+04	1.47E+04	1.47E+04	9.24E+01
30°	1.42E+04	1.64E+04	1.64E+04	1.10E+02

The elastic stiffness coefficients for the Hruska, McConnell and Zemek**,** Machida and Durelli**,** Knapp**,** Kumar and Cochran**,** Sathikh, and Labrosse models are listed in Appendix A.

The axial stiffness $k_{\varepsilon\varepsilon}$, as can be seen in Figure 4.5, is decreasing while the lay angles α are increasing for the finite element model and the analytical models. It can also be seen that all the analytical models except Kumar and Cochran's have coincident results. Kumar and Cochran have accounted for the Poisson ratio effect on geometry in their model, as in the finite element model presented; as a result it can be seen that the analytical model curve and the finite model curve have configurations with different results (percentage), which can be explained by the fact that the element number (24/wire) used for this strand is too small. For lay angle 0° the difference is only 11.03% and as lay angle α increases, the percentage goes up to 22.41% when the lay angle is 30°.

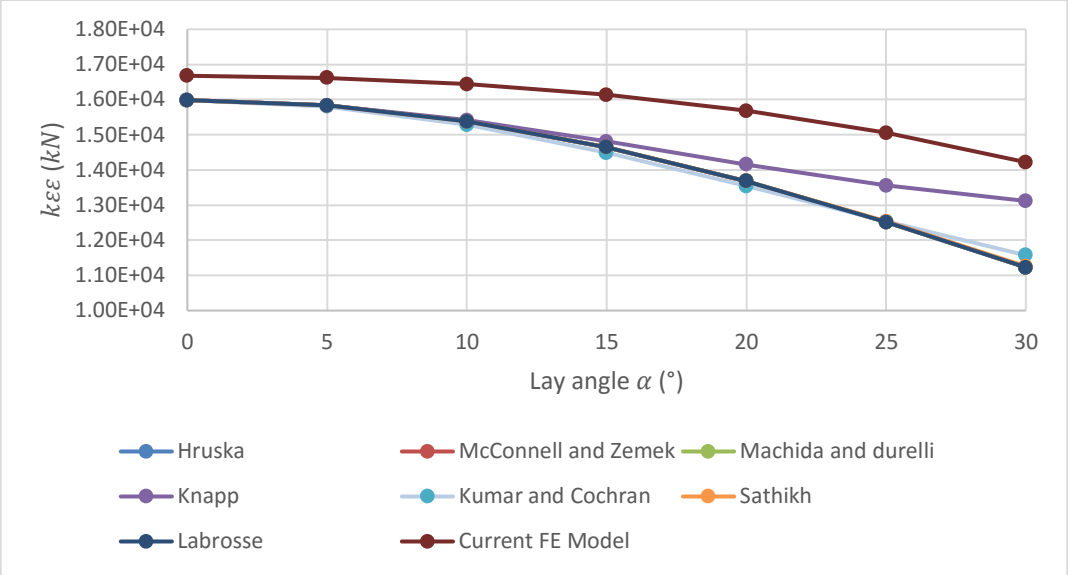

Figure 4.5 Axial stiffness $k_{\varepsilon\varepsilon}$ versus lay angles α.

For both the coupling coefficient terms, between the tensile and the torsional $k_{\varepsilon\theta}$, and $k_{\theta\varepsilon}$ for the finite element, the curve is linearly increasing, as shown in Figure 4.6 and Figure 4.7. It should be noted that, as can be seen in the figures, only Hruska, Sathikh, and Labrosse have a symmetrical matrix beside the proposed finite element model. In addition, similarly to the axial stiffness, in both coupling terms it can be seen that the model which accounted for the Poisson ratio has a result close to the finite element model result. The different percentages between the finite element model and Kumar and Cochran's model for lay angle α, 5°, 20°, and 30° for $k_{\varepsilon\theta}$ is greater by 25.16%, lower by 4.76%, and lower by 3.65%, respectively, and for $k_{\theta\varepsilon}$ is greater by 29.83%, lower by 14.28%, and lower by 3.65%, respectively. And, it can be seen that the Knapp model is also closer to the current model because it added more accurate geometry parameters.

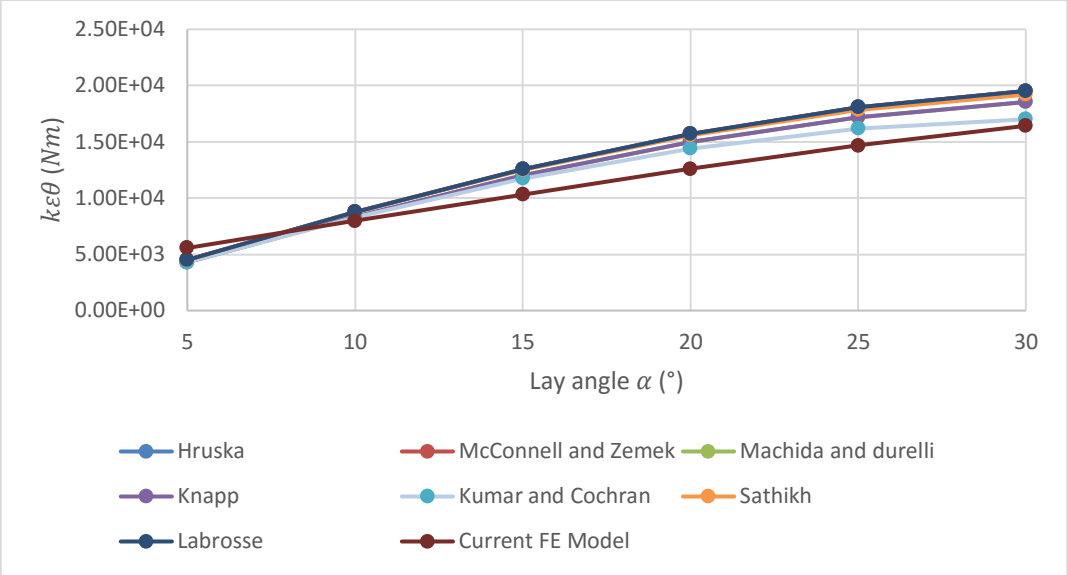

Figure 4.6 Coupling stiffness $k_{\varepsilon\theta}$ versus lay angles α.

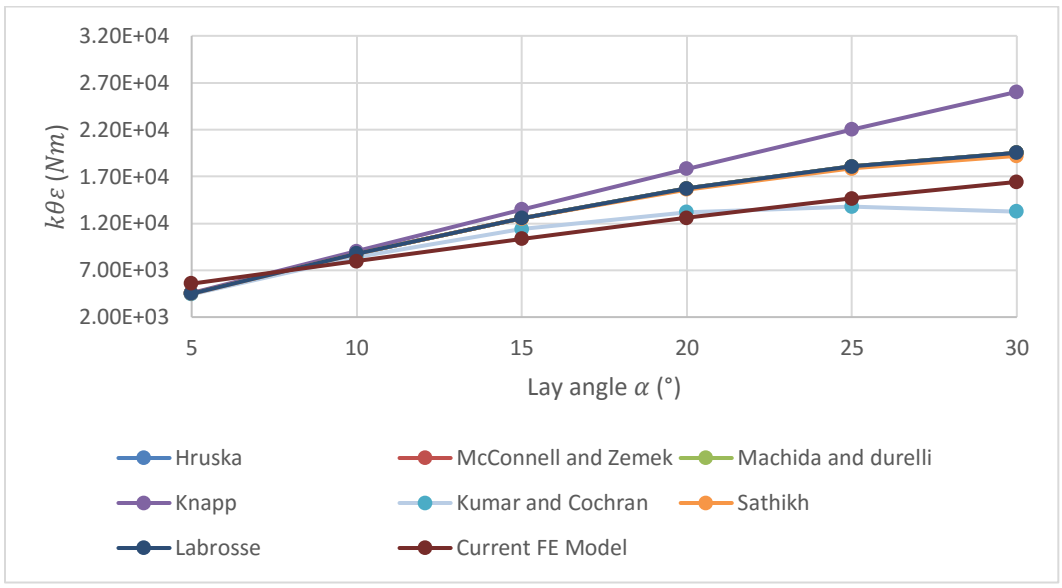

Figure 4.7 Coupling stiffness $k_{\theta\varepsilon}$versus lay angles α.

The torsional stiffness $k_{\theta\theta}$ coefficients also are increasing linearly, as the lay angle is increasing for the current finite element model (Figure 4.8) and in general the result are greater than the analytical models, as in the axial stiffness results. However, the Hurska model has relatively lower values since the torsion was neglected in the model derivation.

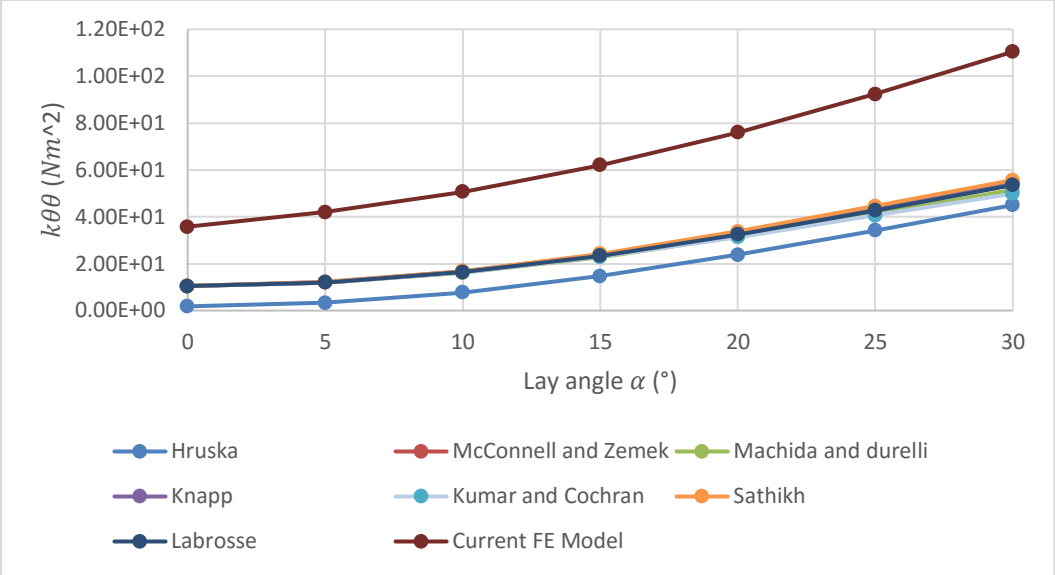

Figure 4.8 Torsional stiffness $k_{\theta\theta}$ versus lay angles α.

4.3 Dynamic Behavior

Free vibration analysis using finite element one-dimensional approximation was performed on the aluminum bar, the trapezoidal wire, and the simple straight strand. The natural frequencies ω and the normal mode shape are presented for each model; for both wires the study was applied for all the lay angles α studied (0°, 5°, 10°, 15°, 20°, 25°, and 30°).

4.3.1 Aluminum Circular Bar

First, the element mass and element stiffness were calculated using equation (3.43) and (3.44), with the following results:

$$m_{cir.\text{alum.}} = \begin{bmatrix} 2.78E-01 & 0.00E+00 & 1.39E-01 & 0.00E+00 \\ 0.00E+00 & 2.73E-05 & 0.00E+00 & 1.36E-05 \\ 1.39E-01 & 0.00E+00 & 2.78E-01 & 0.00E+00 \\ 0.00E+00 & 1.36E-05 & 0.00E+00 & 2.73E-05 \end{bmatrix} \quad (4.1)$$

And:

$$k_{cir.alum.} = \begin{bmatrix} 8.50E+07 & 0.00E+00 & -8.50E+07 & 0.00E+00 \\ 0.00E+00 & 4.16E+03 & 0.00E+00 & -4.16E+03 \\ -8.50E+07 & 0.00E+00 & 8.50E+07 & 0.00E+00 \\ 0.00E+00 & -4.16E+03 & 0.00E+00 & 4.16E+03 \end{bmatrix} \quad (4.2)$$

Then, the accuracy and predictability were checked for the Matlab code and the methodology used for the convergence between the exact solution and the 2, 4, 8, and 16 elements used in the finite element one-dimensional approximation after assembling and applying the boundary conditions where both ends were not allowed either to rotate or extent (fixed-fixed), Table 4.3 shows the known exact axial frequency (equation 3.43) and the torsional frequency (equation 3.44), and from the approximation of 2, 4, 8, and 16 elements, for the first mode. For 2, 4, 8, and 16 elements, the mode shapes were drawn first, so that it will show which frequency is axial or torsional; the normal mode shape is presented later for this uncoupled aluminum bar.

Table 4.3 Axial and torsional frequencies for exact solution and approximate solutions.

Mode 1*	Exact	2 Elements	4 Elements	8 Elements	16 Elements
$\omega_A(\frac{rad}{s})$	1980.52	2182.70	2032.80	1996	1985
$\omega_T(\frac{rad}{s})$	1400.44	1544.40	1437.40	1409	1408

* Where ω_A is the axial frequency and ω_T is the torsional frequency.

It can be seen that the different rates in 2, 4, 8, and 16 are 10.27%, 2.63%, 0.78%, and 0.22%, respectively. This indicates that the 16-element approximation gave excellent results compared with the exact solutions. As a result, the 16-element model was used for this bar and the trapezoidal wire as well as in the simple straight strand.

The natural frequencies ω and the mode shapes were solved using the linear eigenvalues and eigenvector in equation (3.37). Since it is a 16-element bar, 30 frequencies ω were derived, as shown in Table 4.4; to demonstrate which frequency is axial or torsional, the normalized mode

shapes were plotted. In this work, only the first 6 top modes are presented for all the models studied; ω_{un} indicates that the type of this frequency type is unknown.

Table 4.4 The 30 frequencies results for 16-element approximation.

Mode number	Frequency type	Frequency value
1	ω_T	1408
2	ω_A	1985
3	ω_T	2826
4	ω_A	3990
5	ω_T	4269
6	ω_T	5752
7	ω_{un}	6032
8	ω_{un}	7291
9	ω_{un}	8132
10	ω_{un}	8899
11	ω_{un}	10310
12	ω_{un}	10586
13	ω_{un}	12361
14	ω_{un}	12584
15	ω_{un}	14223
16	ω_{un}	14971
17	ω_{un}	16162
18	ω_{un}	17481
19	ω_{un}	18139
20	ω_{un}	20083
21	ω_{un}	20117
22	ω_{un}	21878
23	ω_{un}	22859
24	ω_{un}	23367
25	ω_{un}	24366
26	ω_{un}	25656
27	ω_{un}	28408
28	ω_{un}	30952
29	ω_{un}	33057
30	ω_{un}	34464

As can be shown from Figures 4.9 through 4.14, the normalized modes corresponding to the natural frequencies show that mode 1, mode 3, mode 5, and mode 6 are dominated to be pure

torsion while the extension displacement is zero, and mode 2 and mode 4 are dominated to be pure extension with no torsion displacement. That result indicates that there is no coupling for the aluminum bar.

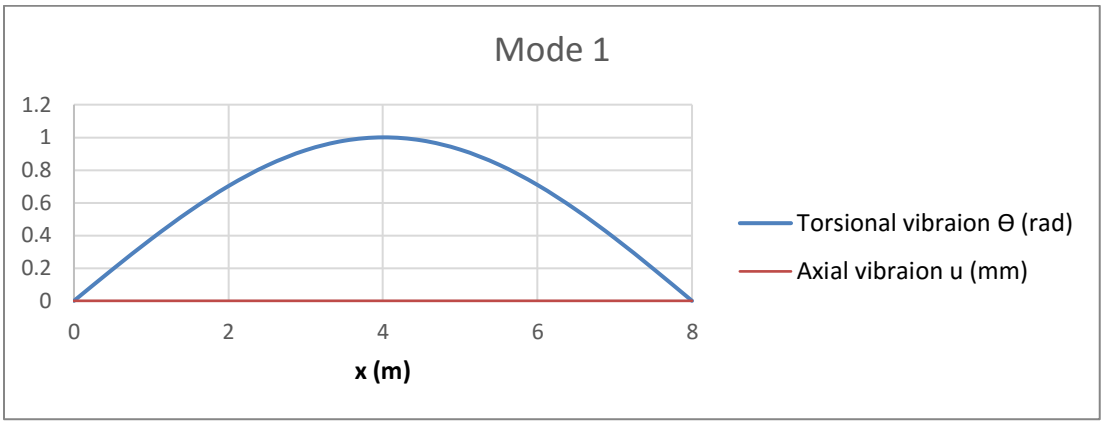

Figure 4.9 First mode for the aluminum bar.

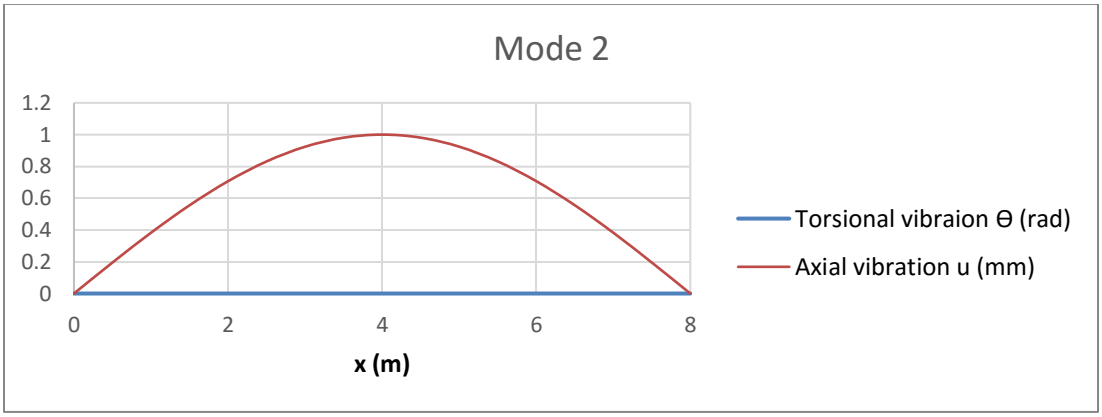

Figure 4.10 Second mode for the aluminum bar.

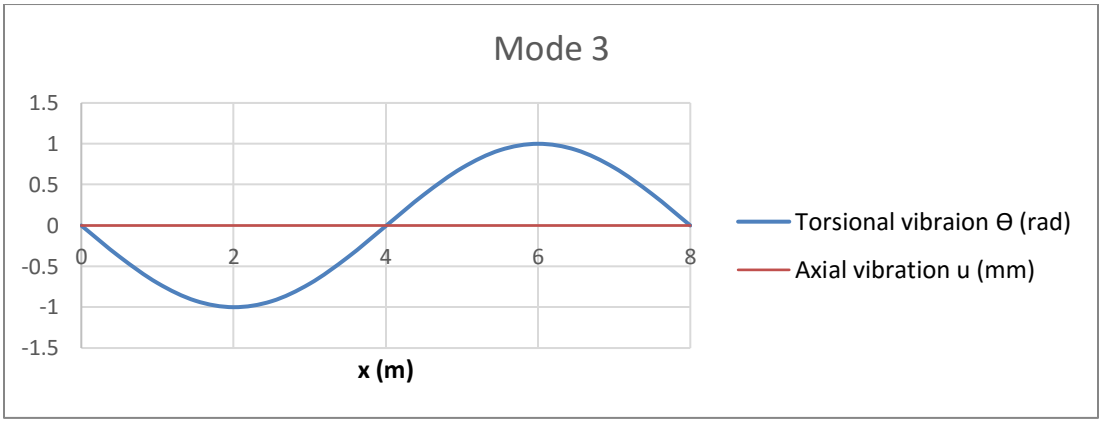

Figure 4.11 Third mode for the aluminum bar.

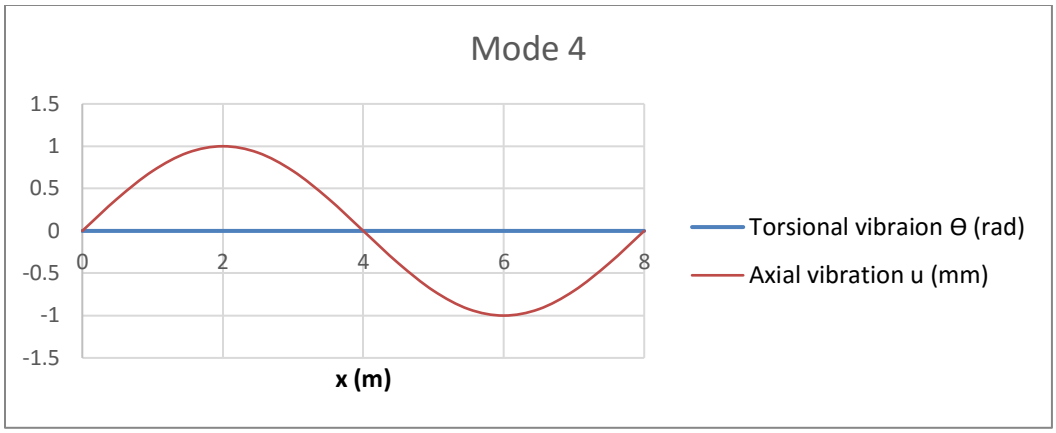

Figure 4.12 Fourth mode for the aluminum bar.

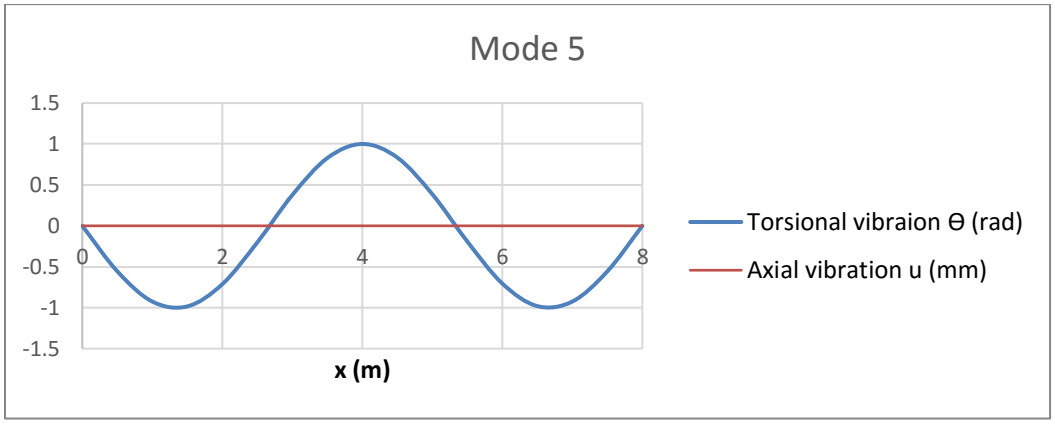

Figure 4.13 Fifth mode for the aluminum bar.

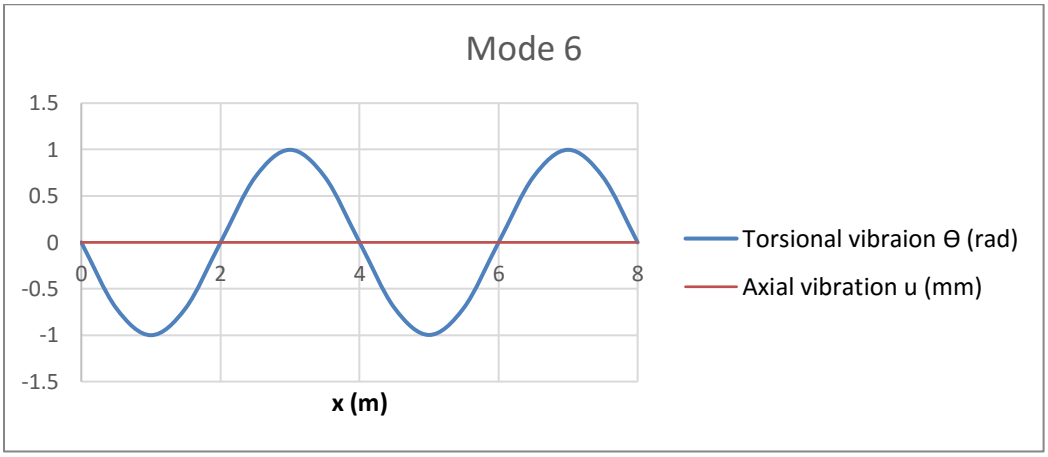

Figure 4.14 Sixth mode for the aluminum bar.

4.3.2 Trapezoidal wire

The natural frequencies and mode shapes for the trapezoidal wire, considering the differences in geometry and material. As described in chapter 3, the element mass $m_{Trap.}$ and stiffness k_α for each lay angle α (0°, 5°, 10°, 15°, 20°, 25°, and 30°) was derived and it can be written as:

$$m_{Trap.} = \begin{bmatrix} 2.57E-01 & 0.00E+00 & 1.28E-01 & 0.00E+00 \\ 0.00E+00 & 2.61E-05 & 0.00E+00 & 1.31E-05 \\ 1.28E-01 & 0.00E+00 & 2.57E-01 & 0.00E+00 \\ 0.00E+00 & 1.31E-05 & 0.00E+00 & 2.61E-05 \end{bmatrix} \quad (4.3)$$

And:

$$k_{\alpha=0°} = \begin{bmatrix} 1.34E+08 & 0.00E+00 & -1.34E+08 & 0.00E+00 \\ 0.00E+00 & 2.71E+03 & 0.00E+00 & -2.71E+03 \\ -1.34E+08 & 0.00E+00 & 1.34E+08 & 0.00E+00 \\ 0.00E+00 & -2.71E+03 & 0.00E+00 & 2.71E+03 \end{bmatrix} \quad (4.4)$$

$$k_{\alpha=5°} = \begin{bmatrix} 1.34E+08 & 1.70E+05 & -1.34E+08 & -1.70E+05 \\ 1.70E+05 & 2.84E+03 & -1.70E+05 & -2.84E+03 \\ -1.34E+08 & -1.70E+05 & 1.34E+08 & 1.70E+05 \\ -1.70E+05 & -2.84E+03 & 1.70E+05 & 2.84E+03 \end{bmatrix} \quad (4.5)$$

$$k_{\alpha=10°} = \begin{bmatrix} 1.33E+08 & 1.85E+05 & -1.33E+08 & -1.85E+05 \\ 1.85E+05 & 2.98E+03 & -1.85E+05 & -2.98E+03 \\ -1.33E+08 & -1.85E+05 & 1.33E+08 & 1.85E+05 \\ -1.85E+05 & -2.98E+03 & 1.85E+05 & 2.98E+03 \end{bmatrix} \quad (4.6)$$

$$k_{\alpha=15°} = \begin{bmatrix} 1.32E+08 & 2.00E+05 & -1.32E+08 & -2.00E+05 \\ 2.00E+05 & 3.14E+03 & -2.00E+05 & -3.14E+03 \\ -1.32E+08 & -2.00E+05 & 1.32E+08 & 2.00E+05 \\ -2.00E+05 & -3.14E+03 & 2.00E+05 & 3.14E+03 \end{bmatrix} \quad (4.7)$$

$$k_{\alpha=20^\circ} = \begin{bmatrix} 1.30E+08 & 2.14E+05 & -1.30E+08 & -2.14E+05 \\ 2.14E+05 & 3.31E+03 & -2.14E+05 & -3.31E+03 \\ -1.30E+08 & -2.14E+05 & 1.30E+08 & 2.14E+05 \\ -2.14E+05 & -3.31E+03 & 2.14E+05 & 3.31E+03 \end{bmatrix} \quad (4.8)$$

$$k_{\alpha=25^\circ} = \begin{bmatrix} 1.28E+08 & 2.28E+05 & -1.28E+08 & -2.28E+05 \\ 2.28E+05 & 3.50E+03 & -2.28E+05 & -3.50E+03 \\ -1.28E+08 & -2.28E+05 & 1.28E+08 & 2.28E+05 \\ -2.28E+05 & -3.50E+03 & 2.28E+05 & 3.50E+03 \end{bmatrix} \quad (4.9)$$

$$k_{\alpha=30^\circ} = \begin{bmatrix} 1.25E+08 & 2.41E+05 & -1.25E+08 & -2.41E+05 \\ 2.41E+05 & 3.71E+03 & -2.41E+05 & -3.71E+03 \\ -1.25E+08 & -2.41E+05 & 1.25E+08 & 2.41E+05 \\ -2.41E+05 & -3.71E+03 & 2.41E+05 & 3.71E+03 \end{bmatrix} \quad (4.10)$$

After finding the element mass and stiffness assembling a 16-element approximation for a trapezoidal wire 8 m in length, and applying the boundary condition (i.e., the wire is fixed at both ends), the eigenproblem was solved using equation (3.37) to find, first, the natural frequencies ω (Table 4.5).

Table 4.5 Natural frequencies for all lay angles for 16-element approximation for trapezoidal wire.

	Natural frequency ω						
Mode	lay angle $\alpha = 0°$	lay angle $\alpha = 5°$	lay angle $\alpha = 10°$	lay angle $\alpha = 15°$	lay angle $\alpha = 20°$	lay angle $\alpha = 25°$	lay angle $\alpha = 30°$
1	1109	1129	1147	1168	1190	1219	1241
2	2229	2267	2304	2347	2390	2445	2491
3	2614	2620	2642	2609	2624	2584	2565
4	3370	3426	3484	3548	3614	3690	3763
5	4544	4618	4696	4783	4871	4970	5070
6	5256	5265	5295	5247	5261	5197	5157
7	5761	5855	5953	6063	6174	6299	6425
8	7032	7146	7266	7400	7536	7687	7799
9	7951	7960	7981	7938	7934	7863	7842
10	8366	8501	8645	8803	8966	9144	9329
11	9769	9927	10095	10280	10469	10602	10515
12	10721	10733	10741	10704	10678	10677	10894
13	11242	11424	11616	11830	12048	12287	12536

14	12775	12981	13200	13442	13528	13441	13331
15	13591	13607	13609	13570	13690	13961	14244
16	14338	14569	14816	15088	15365	15670	15988
17	15878	16133	16406	16563	16510	16406	16271
18	16589	16609	16609	16707	17015	17351	17703
19	17299	17578	17874	18203	18537	18904	19288
20	18476	18773	19090	19441	19639	19519	19358
21	19263	19573	19756	19706	19798	20190	20600
22	19736	19759	19905	20270	20644	21051	21479
23	23045	23072	23064	23010	22928	22792	22604
24	26518	26549	26538	26478	26381	26226	26010
25	30132	30168	30155	30087	29976	29801	29555
26	33820	33858	33843	33769	33644	33448	33172
27	37445	37488	37468	37388	37248	37033	36728
28	40792	40841	40818	40731	40576	40344	40012
29	43568	43619	43596	43503	43339	43090	42734
30	45434	45481	45459	45366	45196	44935	44562

As can be seen in Figure 4.15, the natural frequency ω is increasing linearly (e.g., with 1.80% rate for the first frequencies as the lay angle α is increasing), which indicates that the trapezoidal wire gets stiffer with a higher twist angle.

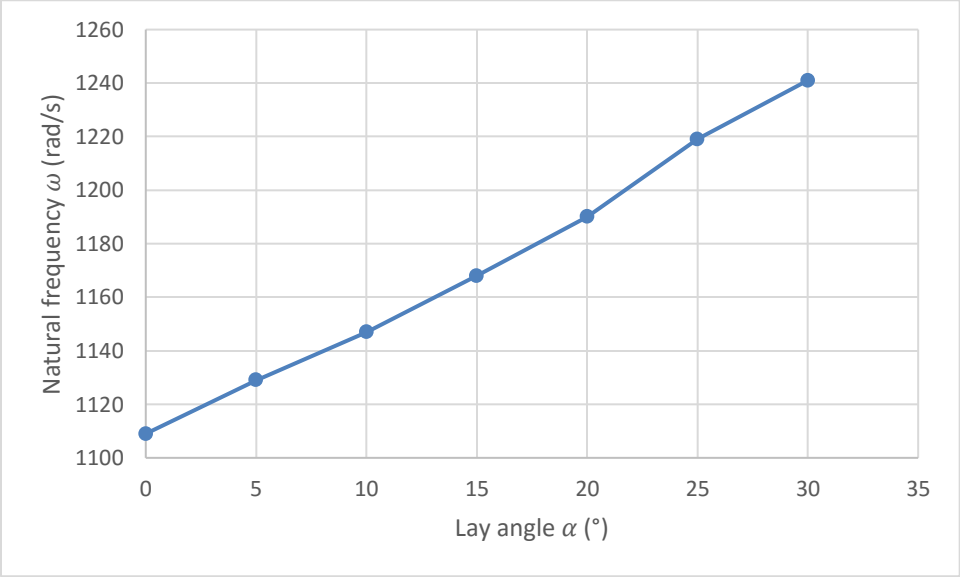

Figure 4.15 Natural frequency ω versus lay angle α for trapazoidal wire.

Second, the top 6 mode shapes of vibration were found from the eigenvectors values from Matlab, showing the interesting extensional and torsional behavior motion of the trapezoidal wire in straight state (0°) with no coupling, and the other case, in which there is a twist in the wire, resulting in a coupled stiffness.

The mode shapes were normalized, and having the 0° lay angle results gave an excellent way to test a frequency and know which one is primarily axial or torsional vibration and then compare it with other vibrations where there are extensional and torsional values for both due to the coupling action in the wire. From Figures 4.16 through 4.21, it can be clearly seen from the 0° lay angle results that: mode 1, mode 2, mode 4, and mode 5 are primarily torsional vibrations, while mode 2 and mode 6 are primarily axial vibrations.

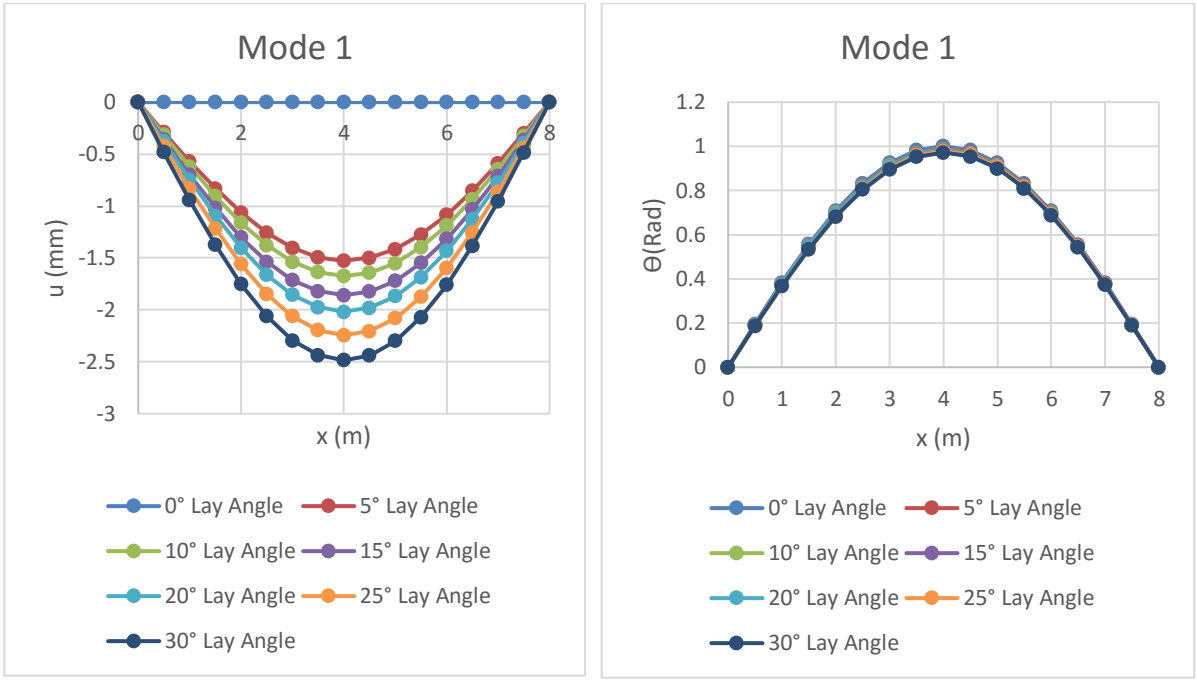

Figure 4.16 First mode for the trapezoidal wire.

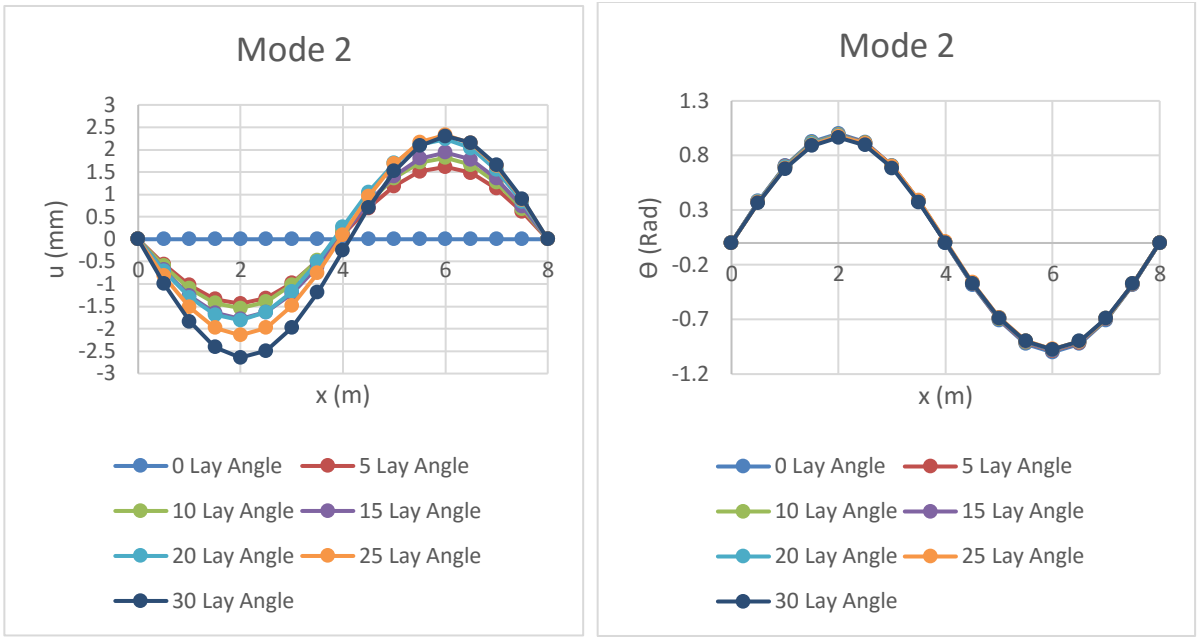

Figure 4.17 Second mode for the trapezoidal wire.

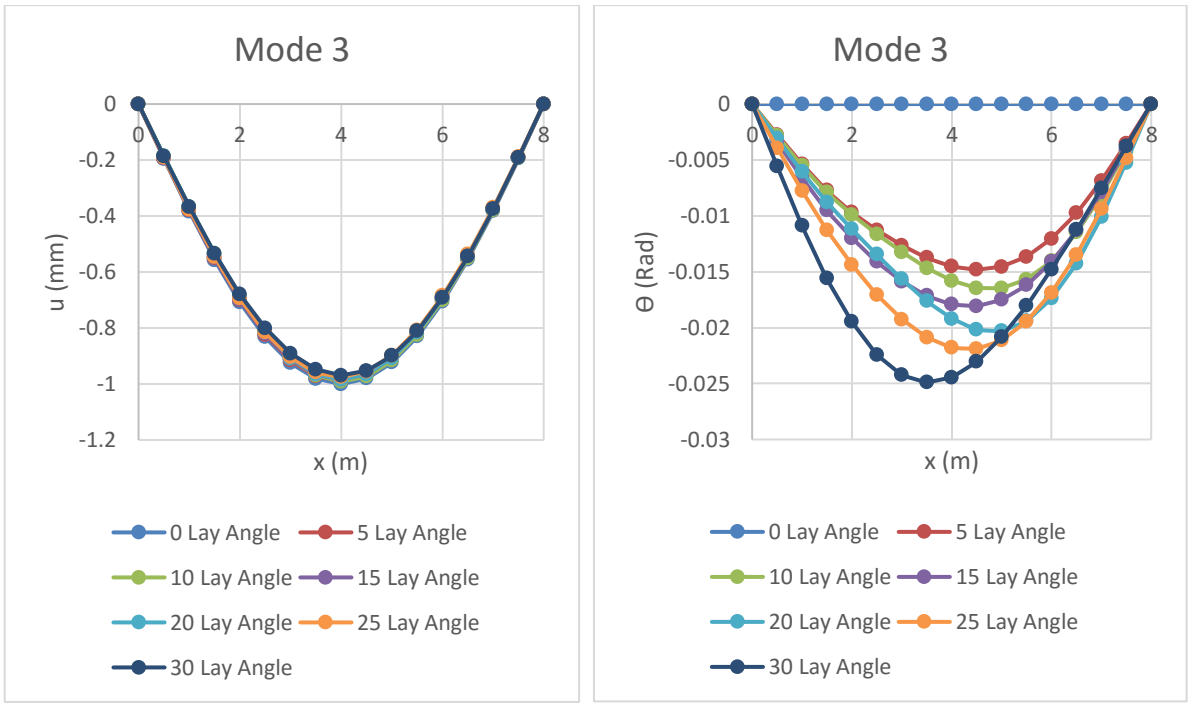

Figure 4.18 Third mode for the trapezoidal wire.

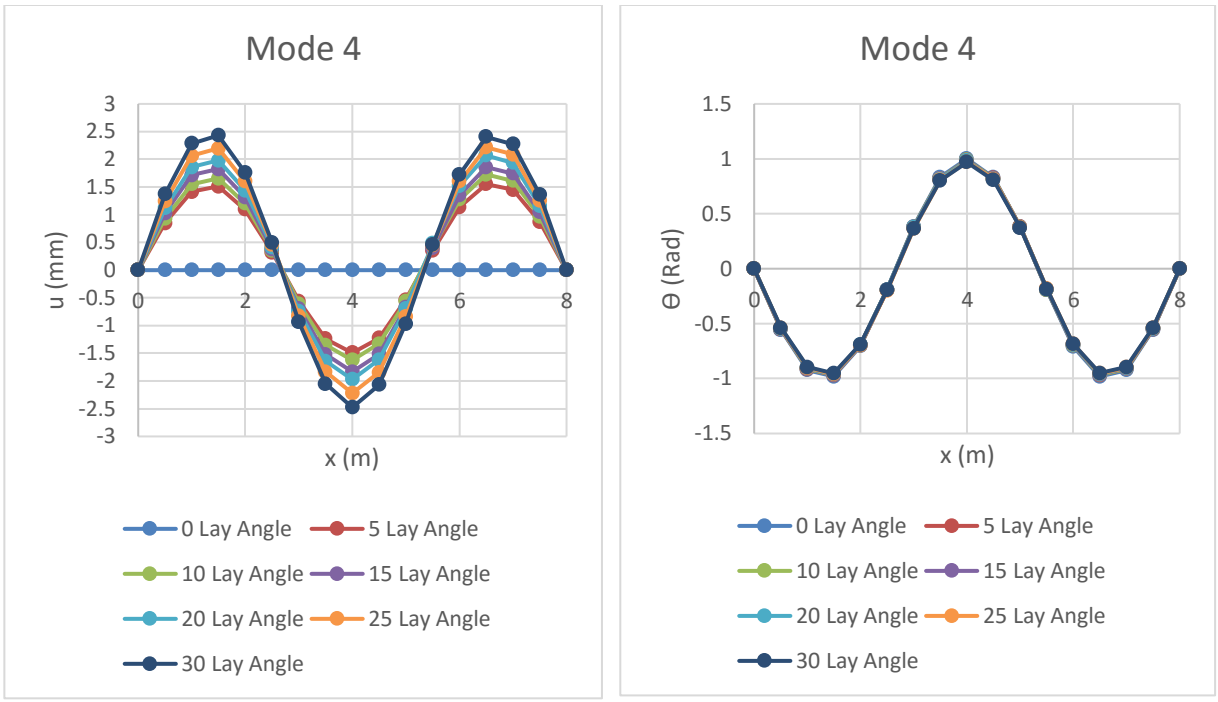

Figure 4.19 Forth mode for the trapezoidal wire.

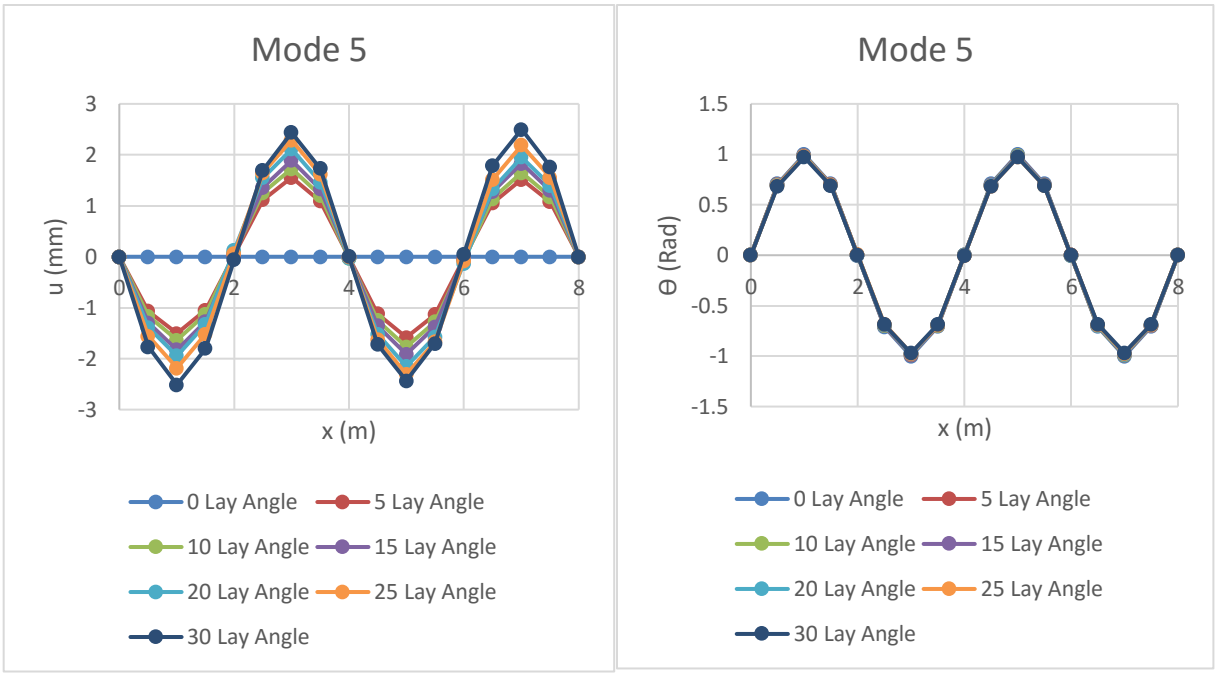

Figure 4.20 Fifth mode for the trapezoidal wire.

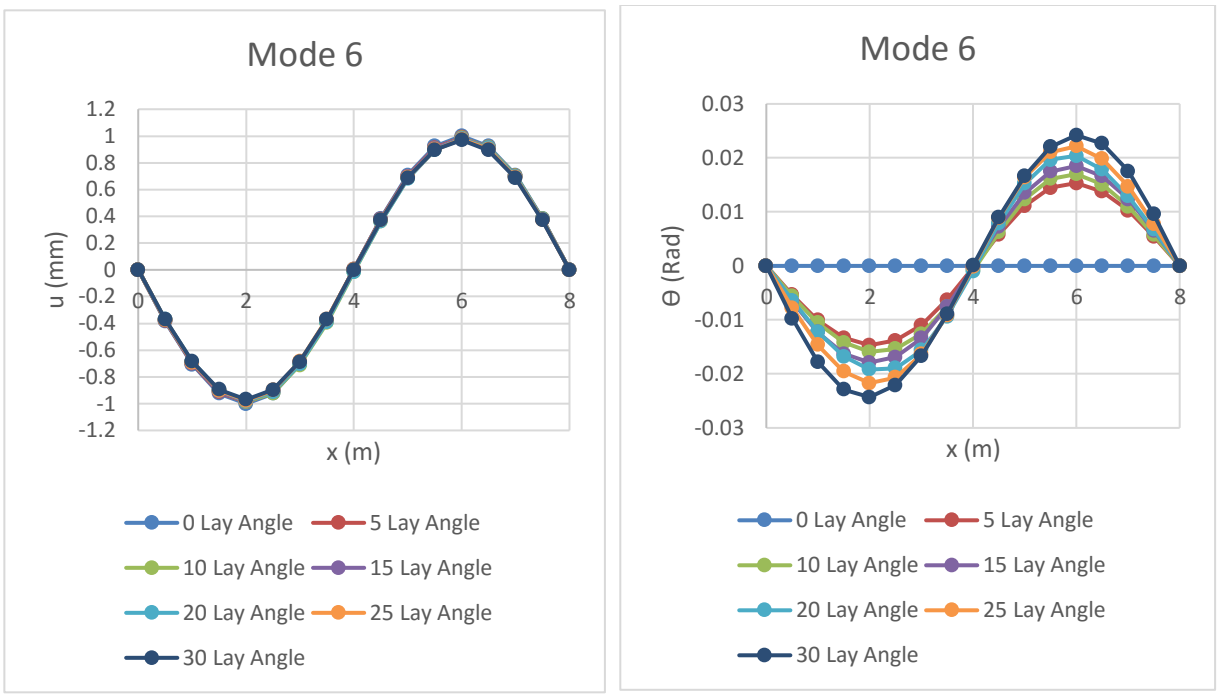

Figure 4.21 Sixth mode for the trapezoidal wire.

Furthermore, as shown here, mode 1, mode 2, mode 4, and mode 5 are primarily torsional vibrations; it also has an axial displacement when the lay angle exists. Mode 1 shows that the peak value of twist Θ at 0° is 1 rad and, once the lay angle α increases, the twist displacement decreases slightly, which represents a very small change in the twist. On the other hand, the axial displacement u at 0° is zero; however, there are axial displacement u values at the same corresponding point, indicating an increase in the axial displacement as the angle increases (see Table 4.6). Modes 2, 4, and 5 have behavior similar to that of the first mode.

Table 4.6 Torsional versus axial values for mode 1 for trapezoidal wire.

Displacements	Mode 1 peak values						
	lay angle $\alpha = 0°$	lay angle $\alpha = 5°$	lay angle $\alpha = 10°$	lay angle $\alpha = 15°$	lay angle $\alpha = 20°$	lay angle $\alpha = 25°$	lay angle $\alpha = 30°$
Torsional Θ (rad)	1	0.990	0.987	0.984	0.981	0.978	0.971
Axial u (mm)	0	1.526	1.672	1.858	2.017	2.244	2.485

For modes (mode 3 and mode 6) which are primarily having axial vibration, in reverse they have torsional vibration. Mode 3 shows that the peak value of axial displacement u is 1 mm, while, with the increase in the lag angle, the displacement value is slightly decreasing as well, proving that only a small change in axial displacement is needed to increase the lay angle; however, the torsional behavior for this mode displays strange values where the peak values shift to the right of the point of symmetry for 5° to 20° , then to the left for 25° to 30° angles. Peak torsional values are listed in Table 4.7. For mode 6, the results were similar to mode 3; however, for the associated torsional values, they were symmetric at the point of symmetry.

Table 4.7 Axial versus torsional values for mode 3 for trapezoidal wire.

Displacements	Mode 3 peak values						
	lay angle $\alpha = 0°$	lay angle $\alpha = 5°$	lay angle $\alpha = 10°$	lay angle $\alpha = 15°$	lay angle $\alpha = 20°$	lay angle $\alpha = 25°$	lay angle $\alpha = 30°$
Axial $u\ (mm)$	1	0.989	0.986	0.983	0.981	0.975	0.968
Torsional $\Theta\ (rad)$	0	0.0148	0.0164	0.0180	0.020	0.021	0.024

4.2.3 Simple Straight Strand

A similar approach was taken to solve the natural frequencies and mode shapes for the simple straight strand, since it has not been solved in the literature. The element mass m_{ss} and stiffness $k_{\alpha}$for each lay angle α (0°, 5°, 10°, 15°, 20°, 25°, and 30°) was derived as indicated in chapter 3 and can be written as:

$$m_{Trap.} = \begin{bmatrix} 9.97E-02 & 0.00E+00 & 4.99E-02 & 0.00E+00 \\ 0.00E+00 & 1.27E-06 & 0.00E+00 & 6.34E-07 \\ 4.99E-02 & 0.00E+00 & 9.97E-02 & 0.00E+00 \\ 0.00E+00 & 6.34E-07 & 0.00E+00 & 1.27E-06 \end{bmatrix} \quad (4.11)$$

And:

$$k_{\alpha=0^\circ} = \begin{bmatrix} 3.34E+07 & 0.00E+00 & -3.34E+07 & 0.00E+00 \\ 0.00E+00 & 7.16E+01 & 0.00E+00 & -7.16E+01 \\ -3.34E+07 & 0.00E+00 & 3.34E+07 & 0.00E+00 \\ 0.00E+00 & -7.16E+01 & 0.00E+00 & 7.16E+01 \end{bmatrix} \quad (4.12)$$

$$k_{\alpha=5^\circ} = \begin{bmatrix} 3.32E+07 & 1.11E+04 & -3.32E+07 & -1.11E+04 \\ 1.11E+04 & 8.39E+01 & -1.11E+04 & -8.39E+01 \\ -3.32E+07 & -1.11E+04 & 3.32E+07 & 1.11E+04 \\ -1.11E+04 & -8.39E+01 & 1.11E+04 & 8.39E+01 \end{bmatrix} \quad (4.13)$$

$$k_{\alpha=10^\circ} = \begin{bmatrix} 3.29E+07 & 1.60E+04 & -3.29E+07 & -1.60E+04 \\ 1.60E+04 & 1.01E+02 & -1.60E+04 & -1.01E+02 \\ -3.29E+07 & -1.60E+04 & 3.29E+07 & 1.60E+04 \\ -1.60E+04 & -1.01E+02 & 1.60E+04 & 1.01E+02 \end{bmatrix} \quad (4.6)$$

$$k_{\alpha=15^\circ} = \begin{bmatrix} 3.23E+07 & 2.07E+04 & -3.23E+07 & -2.07E+04 \\ 2.07E+04 & 1.24E+02 & -2.07E+04 & -1.24E+02 \\ -3.23E+07 & -2.07E+04 & 3.23E+07 & 2.07E+04 \\ -2.07E+04 & -1.24E+02 & 2.07E+04 & 1.24E+02 \end{bmatrix} \quad (4.14)$$

$$k_{\alpha=20^\circ} = \begin{bmatrix} 3.14E+07 & 2.52E+04 & -3.14E+07 & -2.52E+04 \\ 2.52E+04 & 1.52E+02 & -2.52E+04 & -1.52E+02 \\ -3.14E+07 & -2.52E+04 & 3.14E+07 & 2.52E+04 \\ -2.52E+04 & -1.52E+02 & 2.52E+04 & 1.52E+02 \end{bmatrix} \quad (4.15)$$

$$k_{\alpha=25^\circ} = \begin{bmatrix} 3.01E+07 & 2.93E+04 & -3.01E+07 & -2.93E+04 \\ 2.93E+04 & 1.85E+02 & -2.93E+04 & -1.85E+02 \\ -3.01E+07 & -2.93E+04 & 3.01E+07 & 2.93E+04 \\ -2.93E+04 & -1.85E+02 & 2.93E+04 & 1.85E+02 \end{bmatrix} \quad (4.16)$$

$$k_{\alpha=30^\circ} = \begin{bmatrix} 2.84E+07 & 3.28E+04 & -2.84E+07 & -3.28E+04 \\ 3.28E+04 & 2.21E+02 & -3.28E+04 & -2.21E+02 \\ -2.84E+07 & -3.28E+04 & 2.84E+07 & 3.28E+04 \\ -3.28E+04 & -2.21E+02 & 3.28E+04 & 2.21E+02 \end{bmatrix} \quad (4.17)$$

After constructing the element mass and stiffness, the 16-element approximation for simple straight strand (length, 8 m) was assembled; the boundary condition (the wire is fixed at both ends)

was applied, then the eigenproblem was solved using equation (3.37) to find, first, all the 30 natural frequencies ω ; however only the top 6 frequencies are presented in Table 4.8.

Table 4.8 Natural frequencies for all lay angles for 16-element approximation for simple straight strand.

	Natural frequency ω						
Mode	lay angle $\alpha = 0°$	lay angle $\alpha = 5°$	lay angle $\alpha = 10°$	lay angle $\alpha = 15°$	lay angle $\alpha = 20°$	lay angle $\alpha = 25°$	lay angle $\alpha = 30°$
1	850	901	978	1040	1116	1201	1255
2	1711	1809	1958	2078	2079	2445	2093
3	2069	2092	2087	2090	2244	2584	2522
4	2590	2732	2947	3161	3396	3690	3812
5	3494	3682	3961	4182	4184	4970	4203
6	4164	4200	4193	4260	4580	5197	5139

Figure 4.22 shows how the natural frequency ω is increasing at a linear rate of approximately 6%; for example, for the first frequencies the lay angle α is increasing, which indicates that the simple straight strand gets stiffer with a higher twist angle, similarly to the trapezoidal wire.

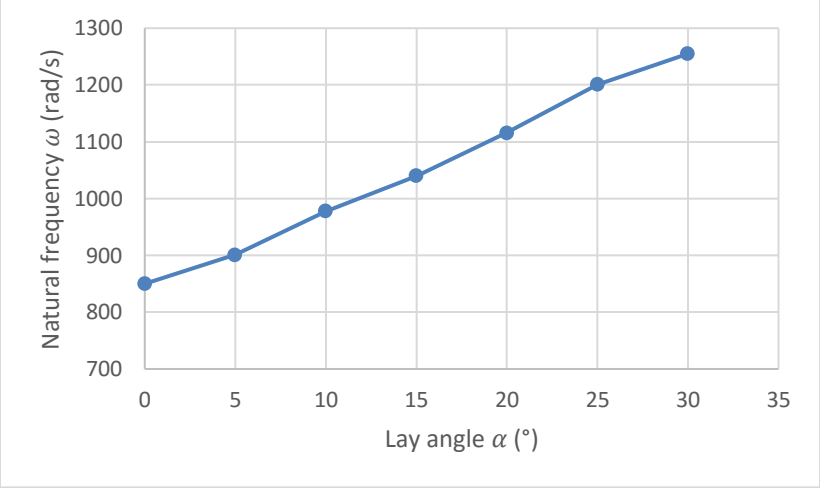

Figure 4.22 Natural frequency ω versus lay angle α for simple straight strand.

Second, extensional and torsional behavior motion of the simple straight strand was studied within the top 6 mode shapes of vibration, which were found using Matlab. The mode shapes were

also normalized, and 0° lay angle results used also as a base to know which one is primarily axial or torsional vibration and then compare it with other vibrations where there are extensional and torsional values for both due to the coupling action in the wire. From Figures 4.23 through 4.28 it can be seen for 0° lay angle (similar to the trapezoidal wire results) that: mode 1, mode 2, mode 4, and mode 5 are primarily torsional vibrations, while mode 2 and mode 6 are primarily axial vibrations.

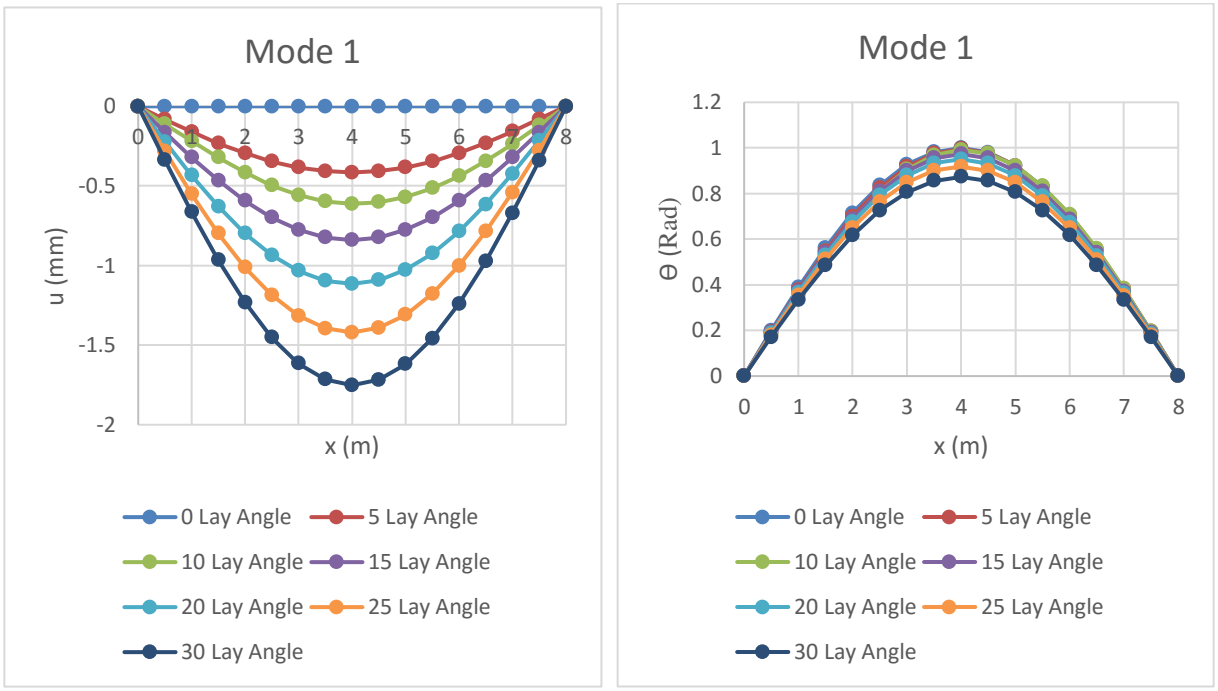

Figure 4.23 First mode for the simple straight strand.

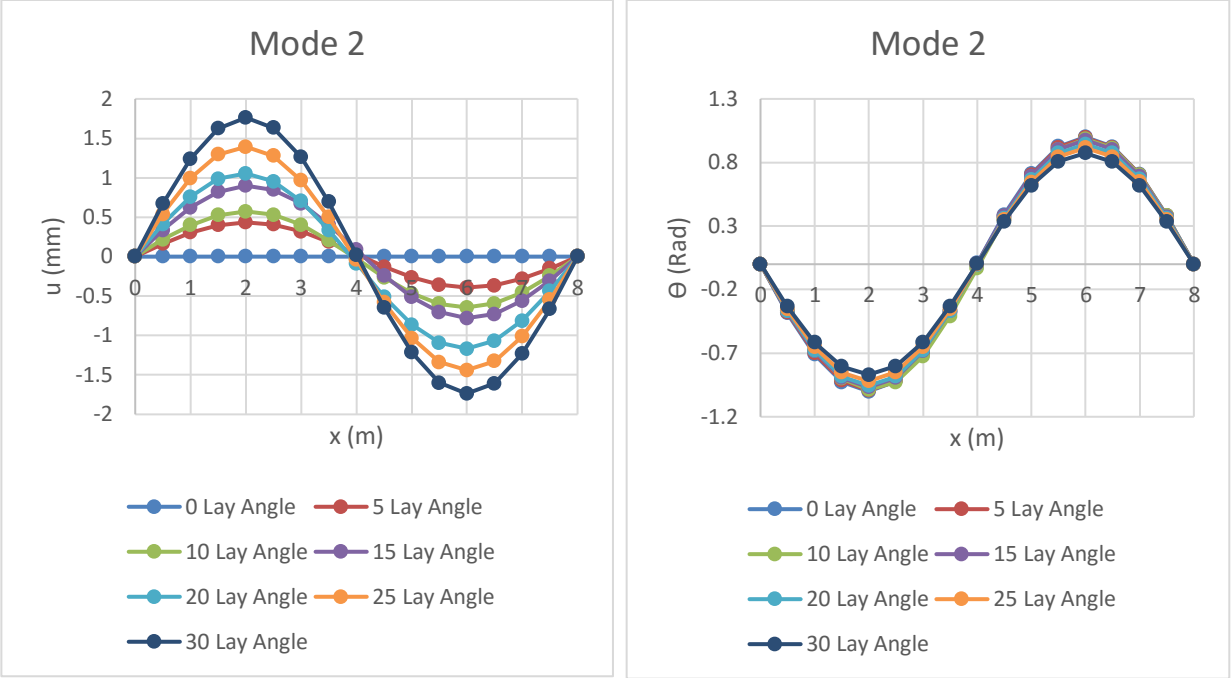

Figure 4.24 Second mode for the simple straight strand.

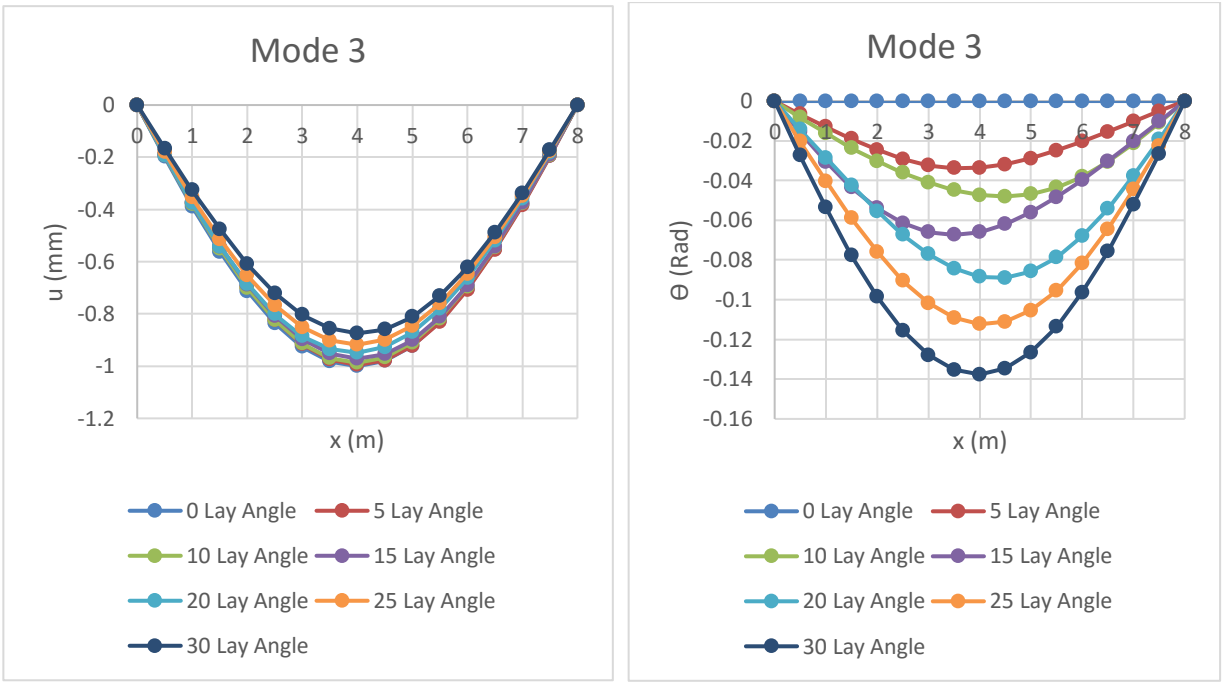

Figure 4.25 Third mode for the simple straight strand.

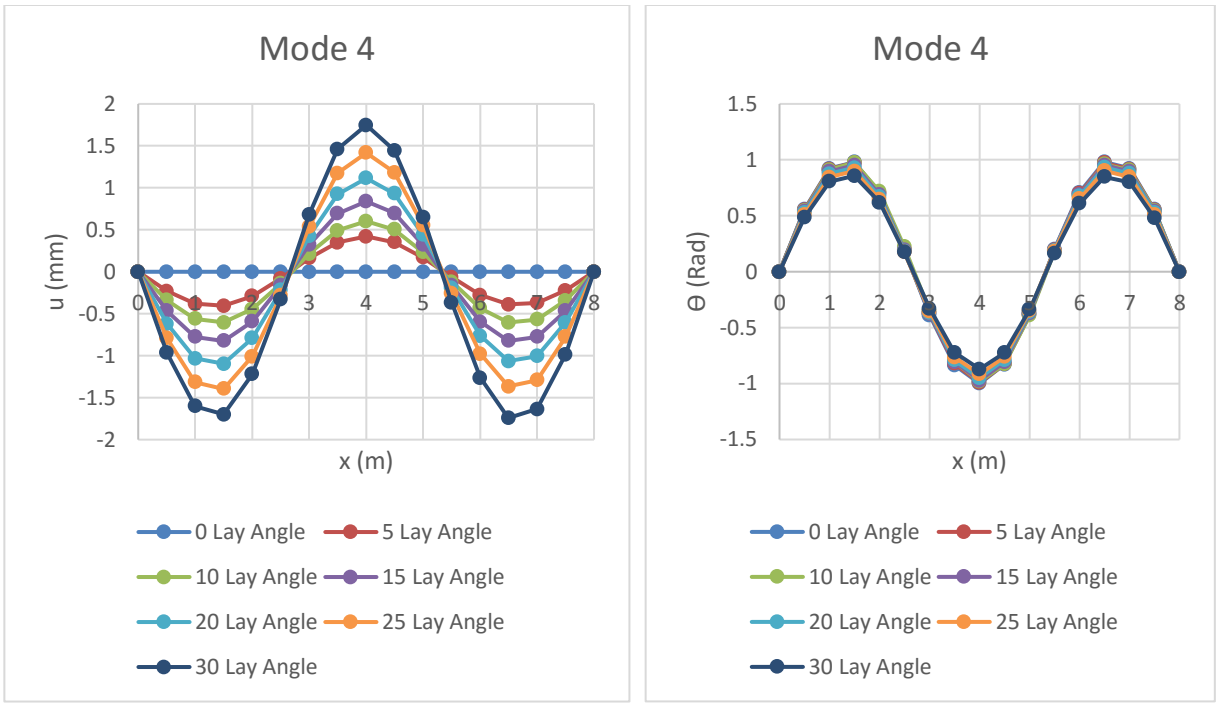

Figure 4.26 Forth mode for the simple straight strand.

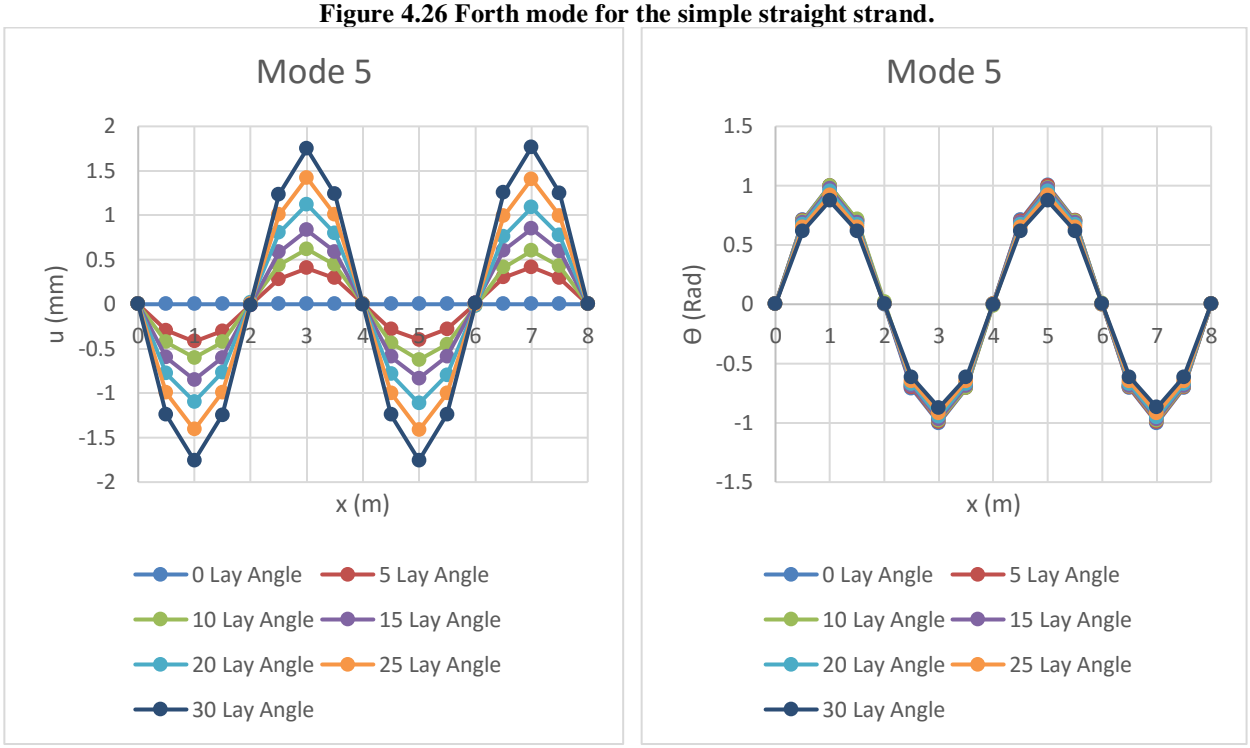

Figure 4.27 Fifth mode for the simple straight strand.

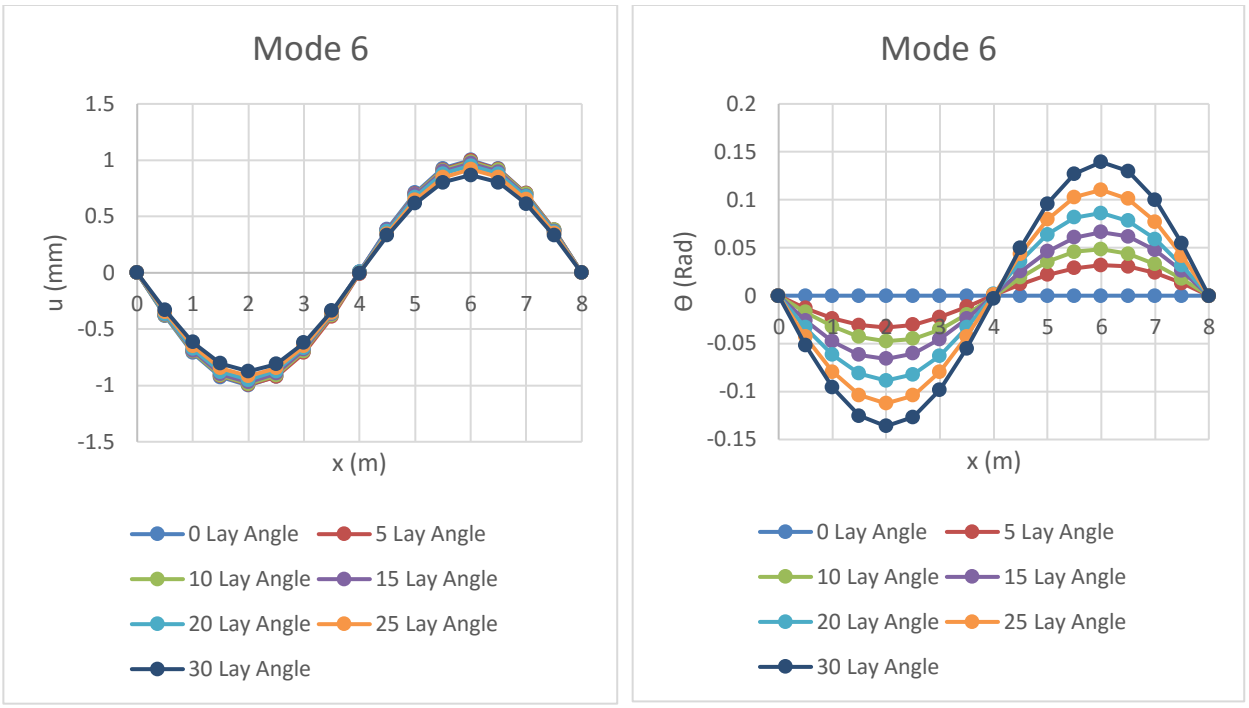

Figure 4.28 Sixth mode for the simple straight strand.

In addition, as indicated previously, mode 1, mode 2, mode 4, and mode 5 are primarily torsional vibrations; it has also an axial displacement when the lay angle exists. Mode 1 shows that the peak value of twist Θ at 0° is 1 rad, and once the lay angle α increases the results indicate a very small change in the twist. On the other hand, the axial displacement u at 0° is zero; however, there are axial displacement u values at the same corresponding point, indicating an increase in the axial displacement as the angle increases (Table 4.9). Mode 2, 4, and 5 have similar behavior to the first mode.

Table 4.9 Torsional versus axial values for mode 1 for simple straight strand.

Displacements	Mode 1 peak values						
	lay angle $\alpha = 0°$	lay angle $\alpha = 5°$	lay angle $\alpha = 10°$	lay angle $\alpha = 15°$	lay angle $\alpha = 20°$	lay angle $\alpha = 25°$	lay angle $\alpha = 30°$
Torsional Θ (rad)	1	0.995	0.991	0.973	0.950	0.918	0.872
Axial u (mm)	0	0.415	0.612	0.840	1.114	1.420	1.751

For mode 3 and mode 6, which are primarily axial vibrations, in reverse they are also having torsional vibration. Mode 3 shows that the peak value of axial displacement u is 1 mm, while the increase in angle indicates that only a small change in axial displacement is needed to increase the lay angle. However, the torsional behavior for this mode displays strange values where the peak values shift to the right then to the left of the point of symmetry for each lay angle change. Peak torsional values are listed in Table 4.10. For mode 6, the results were similar to mode 3; however, for the associated torsional values, they were symmetric at the point of symmetry.

Table 4.10 Axial versus torsional values for mode 3 for simple straight strand.

Displacements	Mode 3 peak values						
	lay angle $\alpha = 0°$	lay angle $\alpha = 5°$	lay angle $\alpha = 10°$	lay angle $\alpha = 15°$	lay angle $\alpha = 20°$	lay angle $\alpha = 25°$	lay angle $\alpha = 30°$
Axial $u\ (mm)$	1	0.995	0.986	0.963	0.948	0.975	0.874
Torsional $\Theta\ (rad)$	0	0.033	0.048	0.067	0.088	0.112	0.137

CHAPTER 5: CONCLUSION

A three-dimensional finite element study was conducted to find mechanical behavior of the new trapezoidal wire and the simple straight wire rope, as part of the validation of the approaches used. A one-dimensional finite element study for free vibration analysis was also done, to study the dynamic behavior of the aluminum bar, the trapezoidal wire, and the simple straight wire.

5.1 Concluding Remarks

As for the elastic behavior of the wires, the trapezoidal wire was studied using three-dimensional finite element Fortran 77 code within 264 elements and 1,590 degrees of freedom for the whole system. The study extended to capture the wire's behavior under varying the lay angles: 0°, 5°, 10°, 15°, 20°, 25°, and 30° where an extensional and torsional coupling action appears in the stiffness matrix due to the existence of the lay angle (twist). Similarly, however, with a smaller element number (24) and a total of 150 degree of freedom for only the outer wire (the core wire was meshed similarly to the simple straight wire rope), it was tested to find the four linear elastic coefficients for all the lay angles studied as well. This model was used to validate the three-dimensional finite element model where this wire has existing analytical models with which it can be compared. The finite element model in comparison with the 7 analytical models gave good estimations, except for Hurska's model (where the torsion effect was ignored), which concluded that the result of a trapezoidal wire's stiffness matrices were valid. The results of the trapezoidal wire were significant where: the maximum axial stiffness value (6.71E+04 kN) at 0° have losted only nearly 7% of the value when it reached the maximum angle used in this study at 30°, the torsional stiffness have increased approximately by 37% when twisted at 30° (1.86E+03 Nm^2), the coupling coefficient terms between the tensile and the torsional are linearly increasing with lay

angle increasing, coupling action will start once the wire has even a small angle twist, the result of a 5° twist for example, indicates that the coupling terms will have a significant value 84.6 kNm compared to no coupling in the straight state (0°). In addition, this is a very important conclusion for designers, which says that this three-dimensional finite element model can be used to estimate the stiffness of a wire where the coupling action can be seen and taken into account.

After solving the axial stiffness for these wires, the free vibration analysis using one-dimensional finite approximation was considered, as it is very important, and to investigate the extensional and torsional coupled stiffness effect on vibration for such structure. As it has not been done before, an aluminum straight bar was analyzed using 2-, 4-, 8-, and 16-element approximation; when the convergence was checked, first it showed that the 16-element approximation gave excellent results, with 0.22% of the exact solutions for the axial and the torsional vibration, so this model was considered for both wires. For trapezoidal wire, the mass matrix required to solve for the eigenvalues (which are the natural frequencies) and the eigenvectors (which are the mode shapes) was computed, and extra care was used due to the complex geometry. Then the vibration was solved and the mode shapes were drawn to see the vibration motion which resulted in finding two types of displacement for each frequency, axial and torsional, at same time for all models (0°, 5°, 10°, 15°, 20°, 25°, and 30°) where there is extensional and torsional coupling behavior. The results were significant where it showed approximately linear increase in the frequency while the lay angle is increasing, which shows that the wire is getting stiffer. In addition, for example, the first mode, which was primarily a torsional vibration, and this displacement goes decreasing with increased of the lay angle; however, it exhibited an axial displacement that increased with the lay angle increase. However, for the sixth mode, which is primarily an axial displacement, it also decreased while the angle increased, and in reverse with

the torsional displacement it increased. The simple straight wire rope behaved similarly to the trapezoidal wire; however, relative to the geometry and material, this wire has lower stiffness and frequencies, and it was tested for all the lay angles studied. In compare of twisted trapezoidal wire and simple straight wire rope's displacements, in the first mode which is dominated to be a torsional vibration, after normalizing the result, the trapezoidal wire displaced 1 rad associated with 2.5 mm, and the simple straight wire rope displaced 1.7 mm; and for the third mode which is dominated to be axial displacement, the trapezoidal wire displaced 0.025 rad in 1 mm, and the simple straight wire rope displaced 0.14 rad for 1 mm. We conclude that it is important to the design, safety, and monitoring, depending on what application these wires are used for, that the coupled frequencies suggested be considered and studied carefully.

5.2 Future Work

In regard to the three-finite element model, for both trapezoidal wire and simple straight wire rope an increase in the finite element number will result in more accurate results in global the stiffness matrix. As well as testing these wires under larger lay angles and investigate their behavior. In addition, the impact of design should be study and that is include: change in the core radius, geometry of the helical, boundary conditions, and the length of the wire. This model can be also developed to include some more nonlinear analysis phenomena, for example, friction, sliding effects, residual stress, elastic-plastic deformation, and contact stress between individual wires within the wire, as this contact can effect all aspects of the wire behavior.

For better understanding of the deformation mechanism of these wires, an increase in number of the one dimensional finite elements model, as well as including a sag to length ratio, and increase the lay angles tested, should increase the accuracy and reality of results of the extensional and torsional free vibration. In addition, finding a quick way to study and investigate

all the values resulting. As well as examine the dynamical responses inform of the natural frequencies and the mode shapes due to wind and seismic loads as forced vibration analysis. Apply same approach used here on the existing wires used in various of engineering applications.

REFERENCES

Alawar, A. A., Bosze, E. J., & R., N. S. (2007). High Temperature Strength and Creep of an Al Conductor with a Hybrid Composite Core. *International Conference on Composite Materials*.

Argatov, I. (2011). Response of a wire rope strand to axial and torsional loads: Asymptotic modeling of the effect of interwire contact deformations. *International Journal of Solids and Structures*, *48*(10), 1413–1423. https://doi.org/10.1016/j.ijsolstr.2011.01.021

Beltran, J. F., Rungamornrat, J., & Williamson, E. B. (n.d.). Computational Model For the Analysis of Damaged Ropes. International Society of Offshore and Polar Engineers.

Beltran, J. F., & Williamson, E. B. (2009). Investigation of the Damage-Dependent Response of Mooring Ropes. *Journal of Engineering Mechanics*, *135*(11), 1237–1247. https://doi.org/10.1061/(ASCE)0733-9399(2009)135:11(1237)

Blouin, F., & Cardou, A. (1989). A study of helically reinforced cylinders under axially symmetric loads and application to strand mathematical modelling. *International Journal of Solids and Structures*, *25*(2), 189–200. https://doi.org/10.1016/0020-7683(89)90006-1

Cardou, A., & Jolicoeur, C. (1997). Mechanical Models of Helical Strands. *Applied Mechanics Reviews*, *50*(1), 1–14. Retrieved from http://dx.doi.org/10.1115/1.3101684

Carlson, A. D., Kasper, R. G., Tucchio, M. A., & LAB., N. U. S. C. N. E. W. L. C. N. E. W. L. (1973). *A Structural Analysis of a Multiconductor Cable*. Defense Technical Information Center. Retrieved from https://books.google.com/books?id=Kzc1OAAACAAJ

Chen, Y., Meng, F., & Gong, X. (2017). Full contact analysis of wire rope strand subjected to varying loads based on semi-analytical method. *International Journal of Solids and Structures*, *117*, 51–66. https://doi.org/10.1016/J.IJSOLSTR.2017.04.004

Chiang, Y. J. (1996). Characterizing simple-stranded wire cables under axial loading. *Finite Elements in Analysis and Design*, *24*(2), 49–66. https://doi.org/10.1016/S0168-874X(97)80001-E

Claude, J., & Alain, C. (1996). Semicontinuous Mathematical Model for Bending of Multilayered Wire Strands. *Journal of Engineering Mechanics*, *122*(7), 643–650. https://doi.org/10.1061/(ASCE)0733-9399(1996)122:7(643)

Costello, G. A. (1978). Analytical investigation of wire rope, *31*(7), 897–900.

Costello, G. A., & JW., P. (1976). Effective Modulus of Twisted Wire Cables. *Journal of the Engineering Mechanics Division*, *102*(1), 171–181.

Crossley, J. A., England, A. H., & Spencer, A. J. M. (2003). Bending and flexure of cylindrically monoclinic elastic cylinders. *International Journal of Solids and Structures*, *40*(25), 6999–7013. https://doi.org/10.1016/S0020-7683(03)00351-2

Crossley, J. A., Spencer, A. J. M., & England, A. H. (2003). Analytical solutions for bending and flexure of helically reinforced cylinders. *International Journal of Solids and Structures*, *40*(4), 777–806. https://doi.org/10.1016/S0020-7683(02)00625-X

Cutchins, M. A., Cochran, J. E., J., Guest, S., Fitz-Coy, N. G., & Tinker, M. L. (1987). An investigation of the damping phenomena in wire rope isolators, *5*, 197–204.

Durville, D. (1998). Modélisation du comportement mécanique de câbles métalliques. *Revue Européenne Des Éléments Finis*, *7*(1–3), 9–22. https://doi.org/10.1080/12506559.1998.11690462

Elata, D., Eshkenazy, R., & Weiss, M. P. (2004). The mechanical behavior of a wire rope with an independent wire rope core. *International Journal of Solids and Structures*, *41*(5–6),

1157–1172. https://doi.org/10.1016/j.ijsolstr.2003.11.021
Erdönmez, C., & Ímrak, C. E. (2009). Modeling and Numerical Analysis of the Strand, *5*(1), 30–38.
Erdönmez, C., & İmrak, C. E. (2011). Modeling Techniques of Nested Helical Structure Based Geometry for Numerical Analysis. *Tehnike Modeliranja Geometrij Na Osnovi Pletenih Vijačnih Struktur Za Numerično Analizo.*, *27*(4), 283–292. Retrieved from http://10.0.21.169/sv-jme.2009.006
Feyrer, K. (2015). *Wire ropes: Tension, endurance, reliability. Wire Ropes: Tension, Endurance, Reliability*. https://doi.org/10.1007/978-3-642-54996-0
Frikha, A., Cartraud, P., & Treyssède, F. (2013). Mechanical modeling of helical structures accounting for translational invariance. Part 1: Static behavior. *International Journal of Solids and Structures*, *50*(9), 1373–1382. https://doi.org/10.1016/j.ijsolstr.2013.01.010
George A. Costello. (1997). *Theory of Wire Ropes* (2nd ed.). Springer-Verlag New York. https://doi.org/10.1007/978-1-4612-1970-5
Ghoreishi, S. R., Cartraud, P., Davies, P., & Messager, T. (2007). Analytical modeling of synthetic fiber ropes subjected to axial loads. Part I: A new continuum model for multilayered fibrous structures. *International Journal of Solids and Structures*, *44*(9), 2924–2942. https://doi.org/10.1016/j.ijsolstr.2006.08.033
Ghoreishi, S. R., Davies, P., Cartraud, P., & Messager, T. (2007). Analytical modeling of synthetic fiber ropes. Part II: A linear elastic model for 1 + 6 fibrous structures. *International Journal of Solids and Structures*, *44*(9), 2943–2960. https://doi.org/10.1016/j.ijsolstr.2006.08.032
Ghoreishi, S. R., Messager, T., Cartraud, P., & Davies, P. (2007). Validity and limitations of linear analytical models for steel wire strands under axial loading, using a 3D FE model. *International Journal of Mechanical Sciences*, *49*(11), 1251–1261. https://doi.org/10.1016/j.ijmecsci.2007.03.014
Hobbs, R. E., & Raoof, M. (1982). Interwire slippage and fatigue prediction in stranded cables for TLP tethers. McGraw Hill.
Hobbs, R. E., & Raoof, M. (1996). Behaviour of cables under dynamic or repeated loading. *Journal of Constructional Steel Research*, *39*(1 SPEC. ISS.), 31–50. https://doi.org/10.1016/0143-974X(96)00028-4
Hruska, F. H. (1952a). Radial forces in wire ropes, *27*(5), 459–463.
Hruska, F. H. (1952b). Tangential forces in wire ropes, *27*(5), 459–463.
Huang, N. C. (1978). Finite Extension of an Elastic Strand With a Central Core. *Journal of Applied Mechanics*, *45*(4), 852–858. Retrieved from http://dx.doi.org/10.1115/1.3424431
Irvine, H. (1974). Studies in the statics and dynamics of simple cable systems.
Jiang, W. (1995). A General Formulation of the Theory of Wire Ropes. *Journal of Applied Mechanics*, *62*(3), 747–755. Retrieved from http://dx.doi.org/10.1115/1.2897010
Jiang, W. G. (2012). A concise finite element model for pure bending analysis of simple wire strand. *International Journal of Mechanical Sciences*, *54*(1), 69–73. https://doi.org/10.1016/j.ijmecsci.2011.09.008
Jiang, W. G., Henshall, J. L., & Walton, J. M. (2000). Concise finite element model for three-layered straight wire rope strand. *International Journal of Mechanical Sciences*, *42*(1), 63–86. https://doi.org/10.1016/S0020-7403(98)00111-8
Jiang, W. G., Warby, M. K., & Henshall, J. L. (2008). Statically indeterminate contacts in axially loaded wire strand. *European Journal of Mechanics, A/Solids*, *27*(1), 69–78.

https://doi.org/10.1016/j.euromechsol.2007.02.003
Jiang, W. G., Yao, M. S., & Walton, J. M. (1999). A concise finite element model for simple straight wire rope strand. *International Journal of Mechanical Sciences*, *41*(2), 143–161. https://doi.org/10.1016/S0020-7403(98)00039-3
Jolicoeur, C. (1997). Comparative study of two semicontinuous models for wire strand analysis.
Jolicoeur, C., & Cardou, A. (1991). A Numerical Comparison of Current Mathematical Models of Twisted Wire Cables Under Axisymmetric Loads. *Journal of Energy Resources Technology*, *113*(4), 241–249. Retrieved from http://dx.doi.org/10.1115/1.2905907
Knapp, R. (1975). Nonlinear analysis of a helically armored cable with nonuniform mechanical properties in tension and torsion. *OCEAN 75 Conference*. https://doi.org/10.1109/OCEANS.1975.1154154
Knapp, R. H. (1979). Derivation of a new stiffness matrix for helically armoured cables considering tension and torsion. *International Journal for Numerical Methods in Engineering*, *14*(4), 515–529. https://doi.org/10.1002/nme.1620140405
Kumar, K., & Botsis, J. (2001). Contact Stresses in Multilayered Strands Under Tension and Torsion. *Journal of Applied Mechanics*, *68*(3), 432. https://doi.org/10.1115/1.1355777
Kumar, K., & Cochran J. E., J. (1987). Closed-Form Analysis for Elastic Deformations of Multilayered Strands. *Journal of Applied Mechanics*, *54*(4), 898–903. Retrieved from http://dx.doi.org/10.1115/1.3173136
Labrosse, M. R. (1998). Contribution à l'étude du rôle du frottement sur le comportement et la durée de vie des câbles monocouches. PhD thesis (in French) - Ecole Centrale de Nantes.
Lee, W. K. (1991). An insight into wire rope geometry. *International Journal of Solids and Structures*, *28*(4), 471–490. https://doi.org/10.1016/0020-7683(91)90060-S
Leech, C. M., Hearle, J. W. S., Overington, M. S., & Banfield, S. J. (1993). Modelling Tension and Torque Properties of Fibre Ropes and splices. *Third (1993) International Offshore and Polar Engineering Conference Singapore, 6-11 June 1993 Modelling*, (June), 6–11.
Lepidi, M., & Gattulli, V. (2012). Static and dynamic response of elastic suspended cables with thermal effects. *International Journal of Solids and Structures*, *49*(9), 1103–1116. https://doi.org/10.1016/J.IJSOLSTR.2012.01.008
Love, A. E. H. (1906). A treatise on the mathematical theory of elasticity. Cambridge: at the University Press. Retrieved from http://hdl.handle.net/10111/UIUCBB:loveau0001tremat
Machida, S., & Durelli, A. J. (1973). Response of a Strand to Axial and Torsional Displacements. *Journal of Mechanical Engineering Science*, *15*(4), 241–251. https://doi.org/10.1243/JMES_JOUR_1973_015_045_02
McConnell, K. G., & Zemke, W. P. (1982). A model to predict the coupled axial torsion properties of ACSR electrical conductors. *Experimental Mechanics*, *22*(7), 237–244. https://doi.org/10.1007/BF02326388
Messager, T., & Cartraud, P. (2008). Homogenization of helical beam-like structures: application to single-walled carbon nanotubes. *Computational Mechanics*, *41*(2), 335–346. https://doi.org/10.1007/s00466-007-0189-3
Michel, L., Anne, N., & Ted, C. (2000). Frictional Dissipation in Axially Loaded Simple Straight Strands. *Journal of Engineering Mechanics*, *126*(6), 641–646. https://doi.org/10.1061/(ASCE)0733-9399(2000)126:6(641)
Mohammed, R., & Ivana, K. (1995). Analysis of Large Diameter Steel Ropes. *Journal of Engineering Mechanics*, *121*(6), 667–675. https://doi.org/10.1061/(ASCE)0733-9399(1995)121:6(667)

Nawrocki, A. (1997). *CONTRIBUTION A LA MODELISATION DES CABLES MONOTORONS PAR ELEMENTS FINIS*. Retrieved from https://books.google.com/books?id=IpzdOgAACAAJ

Nawrocki, A., & Labrosse, M. (2000). A finite element model for simple straight wire rope strands. *Computers & Structures*, *77*(4), 345–359. https://doi.org/10.1016/S0045-7949(00)00026-2

Páczelt, I., & Beleznai, R. (2011). Nonlinear contact-theory for analysis of wire rope strand using high-order approximation in the FEM. *Computers and Structures*, *89*(11–12), 1004–1025. https://doi.org/10.1016/j.compstruc.2011.01.011

Phillips, J. W., & Costello, G. A. (1985). Analysis of Wire Ropes With Internal-Wire-Rope Cores. *Journal of Applied Mechanics*, *52*(3), 510–516. Retrieved from http://dx.doi.org/10.1115/1.3169092

Prawoto, Y., & Mazlan, R. B. (2012). Wire ropes: Computational, mechanical, and metallurgical properties under tension loading. *Computational Materials Science*, *56*, 174–178. https://doi.org/10.1016/j.commatsci.2011.12.034

Ramsey, H. (1988). A theory of thin rods with application to helical constituent wires in cables. *International Journal of Mechanical Sciences*, *30*(8), 559–570. https://doi.org/10.1016/0020-7403(88)90099-9

Ramsey, H. (1990). Analysis of interwire friction in multilayered cables under uniform extension and twisting. *International Journal of Mechanical Sciences*, *32*(8), 709–716. https://doi.org/10.1016/0020-7403(90)90011-7

Raoof, M. (1983). *Interwire contact forces and the static, hysteretic and fatigue properties of multi-layer structural strandsitle*. Imperial Collage of Science and Technology, London, UK.

Raoof, M. (1991). Methods for analysing large spiral strands. *The Journal of Strain Analysis for Engineering Design*, *26*(3), 165–174. https://doi.org/10.1243/03093247V263165

Raoof, M., & Hobbs, R. E. (1988). ANALYSIS OF MULTILAYERED STRUCTURAL STRANDS. *JOURNAL OF ENGINEERING MECHANICS-ASCE*, *114*, 1166–1182. Retrieved from http://gateway.webofknowledge.com/gateway/Gateway.cgi?GWVersion=2&SrcApp=PARTNER_APP&SrcAuth=LinksAMR&KeyUT=WOS:A1988P108400004&DestLinkType=FullRecord&DestApp=ALL_WOS&UsrCustomerID=1ba7043ffcc86c417c072aa74d649202

Raoof, M., & Hobbs, R. E. (1989). TORSIONAL STIFFNESS AND HYSTERESIS IN SPIRAL STRANDS. *Proceedings of the Institution of Civil Engineers*, *87*(4), 501–515. https://doi.org/10.1680/iicep.1989.3775

Raoof, M., & Kraincanic, I. (1994). Critical examination of various approaches used for analysing helical cables. *The Journal of Strain Analysis for Engineering Design*, *29*(1), 43–55. https://doi.org/10.1243/03093247V291043

Raoof, M., & Kraincanic, I. (1995). Simple derivation of the stiffness matrix for axial/torsional coupling of spiral strands. *Computers & Structures*, *55*(4), 589–600. https://doi.org/10.1016/0045-7949(94)00502-T

Rega, G. (2004). Nonlinear vibrations of suspended cables—Part I: Modeling and analysis. *Applied Mechanics Reviews*, *57*(6), 443. https://doi.org/10.1115/1.1777224

Samras, R. K., Skop, R. A., & Milburn, D. A. (1974). An analysis of coupled extensional-torsional oscillations in wire rope. *Journal of Engineering for Industry*, *96*(4), 1130–1135.

Sathikh, S., Moorthy, M. B. K., & Krishnan, M. (1996). A symmetric linear elastic model for

helical wire strands under axisymmetric loads. *The Journal of Strain Analysis for Engineering Design*, *31*(5), 389–399. https://doi.org/10.1243/03093247V315389

Spak, K., Agnes, G., & Inman, D. (2013). Cable Modeling and Internal Damping Developments. *Applied Mechanics Reviews*, *65*(1), 10801–10818. Retrieved from http://dx.doi.org/10.1115/1.4023489

Stanova, E., Fedorko, G., Fabian, M., & Kmet, S. (2011a). Computer modelling of wire strands and ropes Part I: Theory and computer implementation. *Advances in Engineering Software*, *42*(6), 305–315. https://doi.org/10.1016/j.advengsoft.2011.02.008

Stanova, E., Fedorko, G., Fabian, M., & Kmet, S. (2011b). Computer modelling of wire strands and ropes part II: Finite element-based applications. *Advances in Engineering Software*, *42*(6), 322–331. https://doi.org/10.1016/j.advengsoft.2011.02.010

Stanova, E., Fedorko, G., Kmet, S., Molnar, V., & Fabian, M. (2015). Finite element analysis of spiral strands with different shapes subjected to axial loads. *Advances in Engineering Software*, *83*, 45–58. https://doi.org/10.1016/j.advengsoft.2015.01.004

Thai, S., Kim, N.-I., & Lee, J. (2017). Free Vibration Analysis of Cable Structures Using Isogeometric Approach. *International Journal of Computational Methods*, *14*(3), 1750033.

Utting, W. S., & Jones, N. (1987a). The response of wire rope strands to axial tensile loads-Part I. Experimental results and theoretical predictions. *International Journal of Mechanical Sciences*, *29*(9), 605–619. https://doi.org/10.1016/0020-7403(87)90033-6

Utting, W. S., & Jones, N. (1987b). The response of wire rope strands to axial tensile loads—Part II. Comparison of experimental results and theoretical predictions. *International Journal of Mechanical Sciences*, *29*(9), 621–636. https://doi.org/10.1016/0020-7403(87)90034-8

Velinsky, S. A. (1985). General nonlinear theory for complex wire rope. *International Journal of Mechanical Sciences*, *27*(7–8), 497–507. https://doi.org/10.1016/0020-7403(85)90040-2

Wang, D., Zhang, D., Wang, S., & Ge, S. (2012). Finite element analysis of hoisting rope and fretting wear evolution and fatigue life estimation of steel wires. *Engineering Failure Analysis*, *27*, 173–193. https://doi.org/10.1016/j.engfailanal.2012.08.014

Wehking, K., & Zieglen, S. (2004). Calculation of a standard rope with FEM. Wire, *54*(2), 69–100.

Xiang, L., Wang, H. Y., Chen, Y., Guan, Y. J., Wang, Y. L., & Dai, L. H. (2015). Modeling of multi-strand wire ropes subjected to axial tension and torsion loads. *International Journal of Solids and Structures*, *58*, 233–246. https://doi.org/10.1016/j.ijsolstr.2015.01.007

APPENDIX A: THE ELASTIC COEFFICIENTS FOR ANALYTICAL MODELS

The elastic stiffness component for all lay angles studied for Hruska model in Table A.1.

Table A.1 Comparison between the different lay angles matrix components for Hurska model

	Stiffness matrix components			
Lay Angles α	$k_{\varepsilon\varepsilon}(kN)$	$k_{\varepsilon\theta}(Nm)$	$k_{\theta\varepsilon}(Nm)$	$k_{\theta\theta}(Nm^2)$
0°	1.60E+04	0.00E+00	0.00E+00	1.80E+00
5°	1.58E+04	4.50E+03	4.50E+03	3.31E+00
10°	1.54E+04	8.77E+03	8.77E+03	7.73E+00
15°	1.46E+04	1.26E+04	1.26E+04	1.47E+01
20°	1.37E+04	1.57E+04	1.57E+04	2.37E+01
25°	1.25E+04	1.81E+04	1.81E+04	3.41E+01
30°	1.12E+04	1.95E+04	1.95E+04	4.50E+01

The elastic stiffness component for all lay angles studied for McConnell and Zemek model in Table A.2.

Table A.2 Comparison between the different lay angles matrix components for McConnell and Zemek model

	Stiffness matrix components			
Lay Angles α	$k_{\varepsilon\varepsilon}(kN)$	$k_{\varepsilon\theta}(Nm)$	$k_{\theta\varepsilon}(Nm)$	$k_{\theta\theta}(Nm^2)$
0°	1.60E+04	0.00E+00	0.00E+00	1.05E+01
5°	1.58E+04	4.50E+03	4.50E+03	1.20E+01
10°	1.54E+04	8.77E+03	8.77E+03	1.64E+01
15°	1.46E+04	1.26E+04	1.26E+04	2.34E+01
20°	1.37E+04	1.57E+04	1.57E+04	3.24E+01
25°	1.25E+04	1.81E+04	1.81E+04	4.28E+01
30°	1.12E+04	1.95E+04	1.95E+04	5.37E+01

The elastic stiffness component for all lay angles studied for Machida and Durelli model in Table A.3.

Table A.3 Comparison between the different lay angles matrix components for Machida and Durelli model

	Stiffness matrix components			
Lay Angles α	$k_{\varepsilon\varepsilon}(kN)$	$k_{\varepsilon\theta}(Nm)$	$k_{\theta\varepsilon}(Nm)$	$k_{\theta\theta}(Nm^2)$
0°	1.60E+04	0.00E+00	0.00E+00	1.05E+01
5°	1.58E+04	4.50E+03	4.31E+03	1.19E+01
10°	1.54E+04	8.77E+03	8.38E+03	1.62E+01
15°	1.46E+04	1.26E+04	1.20E+04	2.29E+01

20°	1.37E+04	1.57E+04	1.50E+04	3.15E+01
25°	1.25E+04	1.81E+04	1.72E+04	4.13E+01
30°	1.12E+04	1.95E+04	1.85E+04	5.15E+01

The elastic stiffness component for all lay angles studied for Knapp model in Table A.4.

Table A.4 Comparison between the different lay angles matrix components for Knapp model

	Stiffness matrix components			
Lay Angles α	$k_{\varepsilon\varepsilon}(kN)$	$k_{\varepsilon\theta}(Nm)$	$k_{\theta\varepsilon}(Nm)$	$k_{\theta\theta}(Nm^2)$
0°	1.60E+04	0.00E+00	0.00E+00	1.05E+01
5°	1.58E+04	4.54E+03	4.31E+03	1.21E+01
10°	1.54E+04	9.04E+03	8.38E+03	1.67E+01
15°	1.48E+04	1.35E+04	1.20E+04	2.39E+01
20°	1.42E+04	1.78E+04	1.50E+04	3.31E+01
25°	1.36E+04	2.20E+04	1.72E+04	4.36E+01
30°	1.31E+04	2.60E+04	1.85E+04	5.43E+01

The elastic stiffness component for all lay angles studied for Kumar and Cochran model in Table A.5.

Table A.5 Comparison between the different lay angles matrix components for Kumar and Cochran model

	Stiffness matrix components			
Lay Angles α	$k_{\varepsilon\varepsilon}(kN)$	$k_{\varepsilon\theta}(Nm)$	$k_{\theta\varepsilon}(Nm)$	$k_{\theta\theta}(Nm^2)$
0°	1.60E+04	0.00E+00	0.00E+00	1.05E+01
5°	1.58E+04	4.45E+03	4.29E+03	1.20E+01
10°	1.53E+04	8.39E+03	8.30E+03	1.62E+01
15°	1.45E+04	1.14E+04	1.17E+04	2.29E+01
20°	1.35E+04	1.32E+04	1.44E+04	3.13E+01
25°	1.25E+04	1.38E+04	1.62E+04	4.06E+01
30°	1.16E+04	1.33E+04	1.70E+04	4.98E+01

The elastic stiffness component for all lay angles studied for Sathikh model in Table A.6.

Table A.6 Comparison between the different lay angles matrix components for Sathikh model

	Stiffness matrix components			
Lay Angles α	$k_{\varepsilon\varepsilon}(kN)$	$k_{\varepsilon\theta}(Nm)$	$k_{\theta\varepsilon}(Nm)$	$k_{\theta\theta}(Nm^2)$
0°	1.60E+04	0.00E+00	0.00E+00	1.05E+01
5°	1.58E+04	4.50E+03	4.50E+03	1.21E+01
10°	1.54E+04	8.75E+03	8.75E+03	1.68E+01

15°	1.46E+04	1.25E+04	1.25E+04	2.43E+01
20°	1.37E+04	1.56E+04	1.56E+04	3.38E+01
25°	1.25E+04	1.79E+04	1.79E+04	4.45E+01
30°	1.13E+04	1.92E+04	1.92E+04	5.57E+01

The elastic stiffness component for all lay angles studied for Labrosse model in Table A.7.

Table A.7 Comparison between the different lay angles matrix components for Labrosse model

	Stiffness matrix components			
Lay Angles α	$k_{\varepsilon\varepsilon}(kN)$	$k_{\varepsilon\theta}(Nm)$	$k_{\theta\varepsilon}(Nm)$	$k_{\theta\theta}(Nm^2)$
0°	1.60E+04	0.00E+00	0.00E+00	1.05E+01
5°	1.58E+04	4.50E+03	4.50E+03	1.20E+01
10°	1.54E+04	8.77E+03	8.77E+03	1.64E+01
15°	1.46E+04	1.26E+04	1.26E+04	2.34E+01
20°	1.37E+04	1.57E+04	1.57E+04	3.24E+01
25°	1.25E+04	1.81E+04	1.81E+04	4.28E+01
30°	1.12E+04	1.95E+04	1.95E+04	5.35E+01